Masters Thesis

Synthesis and Covalent Surface Modification of Carbon Nanotubes for Preparation of Stablized Nanofluid Suspensions

by

Leron Vandsburger

Department of Chemical Engineering

McGill University

Montréal, Québec, Canada

April 23, 2009

A thesis submitted to McGill University in partial fulfillment of the requirements of the degree of Master of Engineering

Dedication

This report is a summary of work done over the course of two years. It was on the advice of my parents that I undertook it, as it is on their advice that I do almost anything. For that reason, among many others, the work presented herein I dedicate to them.

Acknowledgments

I must acknowledge the advice and supervision of my two advisors, Dr. Sylvain Coulombe and Dr. Jean-Luc Meunier. Their patience, ability, and experience have helped me immeasurably. I feel that I have only just begun to see things clearly, and what I have learned has been through them.

The students of the plasma group have helped me as well. Without the previous work and continuing assistance of Mr. Jason Tavares, Mr. Edward Swanson, and Ms. Carole Baddour, the progress I have made would not have been possible. Other members of the group, while not directly involved in my work, deserve recognition due to their helpful insight and general availability for discussion. These are Martin Lennox, Felipe Aristizabal, Jocelyn Veillieux, and Ramona Pristavita.

The staff members of the Chemical Engineering Department deserve thanks for helping make my project possible. I would like to mention Mr. Frank Caporuscio in particular, for his tireless work on the chemical vapour deposition system. I also wish to acknowledge Dr. David Liu of the McGill Facility for Electon Microscopy (FEMR) for his help in using the transmission electron microscope.

I must acknowledge Mr. Adamo Petosa, for his assistance in using the Z-sizer and the UV-VIS, and Dr. Nathalie Tufenkji for providing those instruments as well as the water contact angle goniometer. Furthermore, Mr. Jeffrey Harvey and Dr. Sasha Omanovic for help in using, and providing, the FTIR microscope.

Finally, all the funding agencies that financed the research work done in the nanofluids group. These are the Natural Sciences and Engineering Research Council of Canada, the Fonds québécois de recherche sur la nature et les technologies, and the Department of Chemical Engineering of McGill University.

Table of Contents

Table of Figures

List of Tables

Abstract

Carbon nanotubes are the current object of fervent research. Their unique properties, including anisotropic heat and electrical conductivities, make them promising candidates for applications ranging from super-thin displays to optimized heat transfer surfaces or polymer-CNT composites. Another application is as a component in a polar nanofluid for use in heat transfer. Numerous studies have reported that including carbon nanotubes in liquids can augment their thermal conductivities greatly, but one great disadvantage of current techniques is their limited applicability to situations of high heat flux or temperature, such as boiling or superheating, respectively. For this to be a possibility, carbon nanotubes must be chemically altered to increase their interaction with polar liquids in a persistent and uniform way.

To that end, this work presents two separate but complementary research efforts. The first is a study on the synthesis of carbon nanotubes by thermal chemical vapour deposition, and the second is on the covalent surface modification of carbon nanotubes for both polar and nonpolar interactions. Ultimately, the goal is the preparation and characterisation of aqueous suspensions of carbon nanotubes. The principal results of the latter study are the successful synthesis of carbon nanotube suspensions that are stable at room temperature, beyond one month after preparation, and in high temperature environments, including boiling, and new information about the effect of radio-frequency plasma treatment in an $Ar/O_2/C_2H_6$ mixture on the surface chemistry of carbon nanotubes.

Abrégé

Les nanotubes de carbone (NTC) font présentement l'objet de plusieurs études. Parmi leurs nombreuses propriétés, les conductivités thermique et électrique des NTC font en sorte qu'ils trouvent des applications dans plusieurs domaines, allant des écrans ultra-minces à des surfaces optimisant les transferts thermiques/électriques, ou comme éléments dispersés formant des polymères conducteurs. De nombreuses études ont démontré que les NTC ont également un avenir prometteur dans les nanofluides. Un nanofluide est une suspension d'objets nanométriques (e.g. nanoparticules, NTC) dans un liquide hôte qui permet le transfert de chaleur avec une meilleure efficacité. En effet, des augmentations importantes de la conductivité de certains liquides hôtes ont été observés suite à la dispersion de NTC. Par contre, l'applicabilité de ces suspensions est remise en question dans des procédés où le fluide serait assujetti à des températures ou des flux de chaleur élevés. Afin de permettre l'usage de nanofluides de NTC dans ces situations, les tubes doivent être modifiés chimiquement pour favoriser leur interaction à long terme avec le liquide hôte.

À cette fin, cet ouvrage présente deux avenues de recherche complémentaires : la synthèse de NTC par dépôt thermo-chimique en phase vapeur et la modification par plasma de la surface de NTC afin d'améliorer l'interaction avec des liquides polaires et non-polaires. Des suspensions aqueuses de NTC ont été préparées et caractérisées. Ces dernières font preuve de stabilité à long terme (plus d'un mois après la synthèse, à température ambiante) et de stabilité thermique (suite à un chauffage important et même l'ébullition). L'effet du traitement par plasma radio fréquence de $Ar/O_2/C_2H_6$ sur la chimie de surface des NTC est également étudié.

1. Introduction

Strongly emphasized in engineering coursework is the importance of efficiency as the only means to minimize waste, whether as energy, mass, or even momentum. In heat transfer applications such as heating, cooling, freezing or boiling, wasted heat or poorly insulated refrigeration lines can have severe economic and environmental repercussions. On the other hand, reduction of waste heat or enhancement of cooling capabilities can salvage the economic feasibility of otherwise doomed processes. Some technologies, such as microprocessors, are actually limited by current methods of heat removal [1]. Industrial methods for increasing the thermal efficiency of common processes require both heat integration techniques and increasing heat exchanger contact area [2]. These are both design stage solutions, and cannot be applied to an operating process without major expense.

Heat transfer in all materials is directly related to electrical conductivity and density (including crystallinity). Crystalline solids tend to conduct heat more readily than amorphous solids, solids more than quiescent liquids, and liquids more than gases [3]. In ordered solids, heat is transferred by a combination of lattice vibrations (phonons) and electron displacements, while in all other materials heat transfer occurs by less orderly collisions [3]. In high temperature processes, molten metals such as sodium can be used to transport heat, but at lower temperatures water or ethylene glycol are more often used [2]. For this reason, it is advantageous to mix solids into liquids to augment the heat transfer properties of coolants. These mixtures are called slurries; and have a composite heat conductivity that is higher than that of the normal liquid. In the original theoretical description, as formulated by J.C. Maxwell in the 19th century [4], the magnitude of the augmentation is inversely related to particle size. This quickly led to the hypothesis that nanoscale particles, which have at least one dimension below 100 nm, would have a significant effect on liquid heat transfer efficiency. As techniques for nanoparticle synthesis advance, the incorporation of nanoscale particles into heat transfer fluids is now possible, forming what are called “nanofluids”.

Recent experimental and theoretical work has stirred much controversy over the potentially considerable effects of nanoparticles, including carbon nanotubes, on the thermal properties of liquids [5-8]. Although the reported effects on properties like thermal conductivity vary greatly, the promise of an increase in heat transfer efficiency warrants the full investigation of nanofluid synthesis and characterization. Unfortunately, due to their typically low surface charge and high surface energy, agglomeration and settling are favoured in suspensions of as-prepared nanoparticles [9]. The augmentation of heat transfer properties ceases as nanoparticles agglomerate into larger macroparticles. Furthermore, macroparticles damage pumping equipment and erode pipe walls. The natural tendency towards flocculation therefore necessitates artificial modification of nanoparticle surface chemistry. The principal methods for stabilization of nanofluids are by covalent, or wet chemical, modification and ionic stabilization using surfactants [7, 10]. Covalent methods change the surface chemical structure of nanoparticles, while ionic methods use dissolved charged species to interact and stabilize the nanoparticles as they are. Regrettably, neither of these techniques is useful for production of a heat transfer nanofluid. Wet chemical functionalization is time and material intensive, while surfactants are not temperature stable.

Carbon nanotube (CNT) suspensions present an especially difficult challenge for both synthesis and stability. As produced, carbon nanotubes (CNTs) are non-polar and have a high aspect ratio [11]. This combination of properties makes them incompatible with polar liquids, which form the vast majority of heat transfer fluids, and greatly increases their propensity to agglomerate and settle. However, CNTs also have the potential to augment heat transport considerably, due to their one dimensional molecular structure [12]. CNT nanofluids have been stabilized using wet chemical functionalization and surfactants, resulting in vulnerability to temperatures above 70°C [9]. More recently, glow discharge treatments have begun to be explored as avenues to functionalize CNTs, in an effort to avoid in-solution functionalization techniques [13]. This is mostly due to agglomeration of CNTs during synthesis, preventing adequate dispersion and uniform functionalization. Such work has not been aimed at the

production of nanofluids, but rather at functionalizing CNTs for purposes such as biocompatibility or nanoporous filtration [14].

The work presented herein comprises two independent efforts, with the common goal of producing a temperature stable CNT nanofluid. The first describes work investigating the growth of CNTs on stainless steel by thermal chemical vapour deposition (t-CVD), and the roles of heat treatment and metal surface grain structure in determining CNT morphology, building on work done by Baddour et al. [15]. The second describes a radio-frequency (RF) glow discharge treatment of CNTs, which was adapted for use with CNTs from work done by Tavares et al. [16], as well as synthesis of nanofluids and characterisaztion of both nanofluids and treated CNT surfaces.

2. Literature Review

2.1 General Background on Carbon Nanotubes (CNTs)

Carbon nanotubes are long self-assembling graphite shell structures that are typically two to three orders of magnitude longer than wide. They have the unique characteristics of strong anisotropy for both heat and electrical conductivity and have an electrical conductivity that is dependent on lattice chirality [11]. Heat conduction is axially preferred and occurs through a mechanism called phonon transfer. A phonon is a quantum of crystal lattice vibration, and is mainly responsible for heat transfer in electrically insulating crystalline solids [12]. In electrically conducting CNTs, heat is also carried by electrons; this further augments the already strong axial heat conductivity [12]. Electrical conductivity is determined by the crystal lattice chiral vector, so a CNT can either be a full conductor or a semiconductor. The number of co-axial walls present in a CNT strongly affects its electrical conductivity, in that multi-walled CNTs are almost always electrically conductive [11]. CNTs can be detected by infra-red spectroscopy, and have a signature absorbance pattern characterized by sp^2 peaks and minimal alkane bends and stretches [17]. CNTs are nonpolar and thus cannot easily be suspended in polar liquids. This has stimulated much research into methods for producing a stable suspension ranging from surface functionalization to advanced surfactants [18]. The unique characteristics of CNTs encourage the pursuit of seemingly countless potential applications. Their dimensions and conductivity promise to make them impressive electron emitters, as SEM electron sources or in super-thin displays [19]. Their strength characteristics have already been put to use in enhanced atomic force microscopes [20]. Their heat conductivity is being investigated for application in heat transfer enhancement in coolants in the present work, and their potential as drug delivery vehicles and small biosensors seems promising [21-23].

2.2 CVD Synthesis Techniques

Numerous methods have been developed thus far to produce carbon nanotubes. Among them are arc discharge [11, 24], laser ablation [25, 26], and chemical vapor deposition (CVD) [27, 28]. CVD has the advantage over the previously mentioned methods, as it produces more uniform tubes with less amorphous by-product [11]. The general procedure for CVD begins by preparing a substrate. This preparation typically involves coating a silicon or metal substrate with a thin film of iron or nickel, then using either heat or laser treatments to crack the film into nanoscopic "islands"[29]. Transition metals are preferred due to their carbon solubility characteristics. The resulting substrate is thus coated with metal nanoparticles. One experiment in particular used a thin film of ferrocene deposited on stainless steel [30]. After preparation, the thermal CVD synthesis procedure begins by placing the substrates in a tubular furnace. The experiment takes place in a controlled atmosphere, to prevent oxidation of carbon at high temperature. This is achieved by using a quartz tube with an inert gas atmosphere. The furnace is heated to a temperature between 500-1000 ^{o}C, and a hydrocarbon gas is passed through the reaction chamber [29]. Depending on the gas used, the CNT type can be controlled. Ethylene or acetylene gases for example, produce MWNTs, while methane gas at elevated temperatures has been shown to produce SWNTs [11, 28]. At the catalyst surface, the hydrocarbon gas decomposes into carbon and hydrogen and the carbon dissolves into the metal. An additional technique has been developed, where a plasma discharge is created in the reaction chamber. Strong electric fields and high surface energy have been found to accelerate and align the growth of CNTs with the field, so the technique is called plasma enhanced CVD, or PECVD[31].

Unfortunately, the deposition of iron nanoparticle "catalysts" onto silicon substrates now required by conventional CVD methods is not perfect [11]. Iron nanoparticles are difficult to produce and their deposition is inefficient. Furthermore, iron catalyst nanoparticles are often weakly attached to the substrate, and become incorporated into CNT ends. This is a considerable problem for separation and purification, often requiring an additional wet chemical acid etching step [11]. For these reasons, despite the usefulness of catalyst

deposition in creating precise arrangements of single CNTs through nanolithography [31], alternatives have been devised to eliminate the need for iron catalyst nanoparticles. To avoid these problems, "catalyst-less" CVD methods have been developed wherein stainless steel samples are treated to an adapted CVD procedure to grow MWNTs [15, 32]. Rather than depositing iron nanoparticles on a silicon substrate as before, this method uses the iron in the stainless steel as the catalyst, and requires only a simple etching treatment in acid to reduce the native oxide layer. This method is described in full in the experimental methods section of this work. Although the effectiveness of this method has been established, what role the components of the steel play in the formation of carbon nanotubes is still undetermined.

2.3 304 Stainless Steel Grain Development and Sensitization

Austenitic stainless steel is an alloy of primarily iron (Fe), chromium (Cr), carbon (C), and nickel (Ni). The composition by mass of most 300 series stainless steels is around 18% Cr, .08% C, 10% Ni, and the remainder Fe, with trace amounts of Mn, Si, P, and S [33]. 304 series stainless steel in particular is the most widely used type. It is used in machinery, piping, and in the food industry. It can be polished to a mirror finish, and is non-magnetic, even at cryogenic temperatures [33]. The grain structure of 304 steel is dependent on the type of work that has been done, but it does not lose its properties after hot or cold working. Typically, cold working leads to smaller grains, while hot working or annealing causes the steel to form larger grains. Because of its high chromium content, 304 series stainless steel is susceptible to carbide formation at high temperatures. This has a negative effect on the corrosion properties of the stainless steel [34].

In austenitic stainless steels of the 300 series, carbides form between 650°C and 850°C. They begin to form after as little as 15 min within the aforementioned temperature range and their precipitation is strongly affected by the cooling rate [33]. Chromium carbides precipitate at high energy sites in the metal lattice, most typically at grain boundaries or dislocations but also at interstitial defects, and are much richer in chromium than the surrounding steel. This causes precipitating nuclei to draw chromium out of the matrix, leaving chromium depleted zones around each nucleus [35]. These depleted zones become corrosion sensitive because

they are essentially exposed iron and nickel. The term used to describe such susceptibility to inter-granular corrosion is *sensitization* [34, 35].

It has been reported that the average size of surface grains directly affects the sensitivity of stainless steels [36-39]. The implication being that with increasing grain size, larger chromium depletion zones develop. This is due to the interaction of two major factors. In competition with the formation of chromium depleted zones is a phenomenon called desensitization, whereby chromium diffuses along grain boundaries to equalize the chromium concentration in the steel matrix and restore the chromium passive layer [35]. With increasing grain size, diffusion ceases to be adequate to allow for desensitization, and chromium no longer passivates exposed regions. The general effect of grain size on carbide precipitation is that at small grain sizes, carbides do not cause intergranular corrosion due to desensitization, but at larger grain sizes, desensitization does not hinder the development of depleted zones, and pitting occurs. At large enough grain size, chromium carbides form a coherent network of sensitized zones that form along grain boundaries, and significantly weaken the structural properties of the steel [36].

2.4 CNT Functionalization

The unique electronic and crystal properties of carbon nanotubes have not only generated strong interest in synthesis techniques, but have also spurred investigation into applications of CNT properties. Unfortunately, CNTs in pure form are unreactive, tend to agglomerate in both polar and nonpolar liquids, and are difficult to manipulate [40-43]. To facilitate the use of CNTs in ways that would ordinarily be difficult, many approaches have been proposed, and successfully demonstrated, to attach surface modifying groups to the basic graphene CNT lattice [44-48]. The primary approaches to date have modified CNTs in five ways; altering the sp^2 structure to augment reactivity through production of defects by heating or other oxidation, covalent bonding of functional groups, intermolecular bonding of polymers or other functional molecules, and containment of groups within CNTs [13, 44]. For example, a two stage process to stablize CNTs in non-polar solvent first fluorinates the tubes, suspends them in an organic liquid, then de-fluorinates and alkylates them, by gringard reaction or

otherwise. The goal of the approach is to provide the CNTs with nonpolar surface groups to produce a stable solution of nanotubes in numerous organic solvents [45, 48] Another approach uses non-covalent addition of surfactant molecules to augment CNT surface activity. Stable micellar dispersions have been formed using ionic organic surfactants such as benzalkonium chloride [49]. One article describes an exhaustive examination of the effect of tens of surfactants in as many solvents [50]. Unfortunately, surfactant-stabilized solutions are known to break down at high temperatures [18]. This limits the applicability of non-covalent modification of CNTs for heat transfer application. Biopolymer addition is particularly interesting as a possible process for the synthesis of CNT-biomolecule composite sensors or highly selective drug delivery vehicles [51, 52]. Biopolymers diminish the heat transfer properties of CNTs, so the approach is inapplicable to the present work.

Plasma functionalization is particularly important to the present work, so it is discussed in detail. In general, the energized species in plasma allow reactions to occur that would be thermodynamically disfavored at reactor temperatures and pressures. Functionalization occurs when radical or energized groups in the plasma react with CNTs to form covalent bonds [14, 53-57]. This alters the hybrid orbital structure of CNTs, and causes increased activity such as high reactivity or enhanced intermolecular bonding. The graphene surfaces of CNTs undergo addition reactions, adding highly energized hydroxyl or other polar oxygen groups from the gas. CNTs retain these surface groups after the plasma treatment has concluded, and display elevated hydrophilicity [14, 54, 58]. Polar functional groups have been added successfully to CNTs via plasma treatments. One study reported that a 13.5 MHz RF plasma of pure oxygen can attach polar functional groups, such as hydroxyls, carbonyls, and carboxylics through reactive opening of the CNT lattice, by varying the plasma power, gas pressure, and substrate position relative to the RF electrodes [53].

There have been no studies yet published reporting the use of non-thermal plasma to produce aqueous CNT nanofluids, but numerous studies have investigated the surface activity of plasma treated CNTs. Most work has focused on pure gases, and low pressure (*.05 torr*) [53, 54, 59], but mixtures of oxygen and fluorinated gases have also been reported [55, 60].

Studies have also reported successful deposition of polystyrene onto carbon nanofibers [61] and pyrrole onto CNTs [62]. Nitrogen has been used to incorporate amines and amides into CNT lattices [59]. Several of the previously mentioned studies have reported successful hydrophylization of CNTs, but they do not address the stability of the surface change, and neglect to mention hydrophobic recovery [14, 58], whereby a functionalized surface ceases to show hydrophilic behaviour after time [63].

2.5 Nanofluid Stability and Preparation

At the scale of suspended nanoparticles, body forces such as buoyancy and gravity no longer affect suspension stability. Instead, stochastic motion, also known as Brownian motion, dominates, allowing nanoparticles to remain suspended if intermolecular forces make it favourable [64]. In most nanofluid suspensions, nanoscale particles are thermodynamically likely to agglomerate and settle due to increased van der Waals bonding [65]. Van der Waals forces result from temporary electric dipole moment interactions that randomly and transiently couple two molecules together. This force will cause settling in nanofluids, because there is often little interaction between the liquid and suspended nanoparticles, making suspended nanoparticles favor each other [5]. As nanoparticles agglomerate, the force of gravity becomes significant and forces the particles to settle out of solution. In most stable nanofluids, the nanoparticles have been chemically or physically altered to produce a favourable interaction with the liquid it is suspended in. For nonpolar liquids, this could entail non-covalent polymer coating or covalent attachment of nonpolar surface groups. For polar liquids, it requires attachment of polar surface groups either by noncovalent polar polymer coating, or covalent oxidation or nitration. These have both been previously discussed.

Another option is to alter the liquid to promote its interaction with suspended nanoparticles. This typically means adding an ionic surfactant or adjusting the pH to increase the electrolytic activity of the liquid [66].

Nanofluids are typically produced by mixing commercially prepared nanoparticles in a liquid using a sonic bath or sonicator [18]. This method is usually unsuccessful without some prior nanoparticle surface treatment, because commercially prepared nanoparticles are always

agglomerated and their composition is difficult to control. Other methods involve wet chemical precipitation and gas phase condensation, but these will not be discussed here. Commercially prepared CNT suspensions are available, but these are all stabilized by addition of ionic surfactants, and no work has yet been reported on the preparation of stable aqueous CNT suspensions that do not include surfactants. Furthermore, CNT nanofluids capable of withstanding boiling temperatures have not yet been produced.

3. Objectives

For the investigation of t-CVD synthesis of CNTs, the main project objectives were:

1. **To grow CNTs using three heat treatment protocols adapted from the standard t-CVD method**
2. **To characterize the resulting CNT morphologies, with regard to suitability for subsequent RF plasma treatment**

In the second section of this Masters work relating to surface functionalization of CNTs and nanofluid synthesis, the objectives are as follow:

1. **To develop a method to produce aqueous CNT nanofluids**
2. **To characterize the CNT nanofluids**

4. Experimental Methods

4.1Thermal-CVD Reactor

The reactor assembly used to synthesize CNTs consists of a gas supply system, a resistive high temperature furnace, a quartz tube, and an exhaust apparatus. A diagram of the setup is shown in Figure 1. Two Brooks model 5850E mass flow controllers maintain the flow rates at the desired setpoints. The resistive furnace is a Lindberg/Blue HTF 55000 series $(120\ V/30\ A)$. The reaction takes place within a quartz tube $(\phi = 5.5\ cm,\ l = 121.9\ cm)$. The quartz tube is flanged on either end and is sealed before each experiment using a set of flanged end caps. The quartz tube was purchased from Technical Glass Products, USA, while the flanged end pieces and end caps were purchased from EVAC vacuum company, Switzerland. The inert carrier gas is nitrogen (N_2) and the carbon source gas is acetylene (C_2H_2). The gases are injected into the quartz tube through a smaller quartz inlet tube $(\phi = 6.35\ mm)$ that extends into the high temperature region. The gases finally exit through a stainless steel endpipe that leads to the exhaust system.

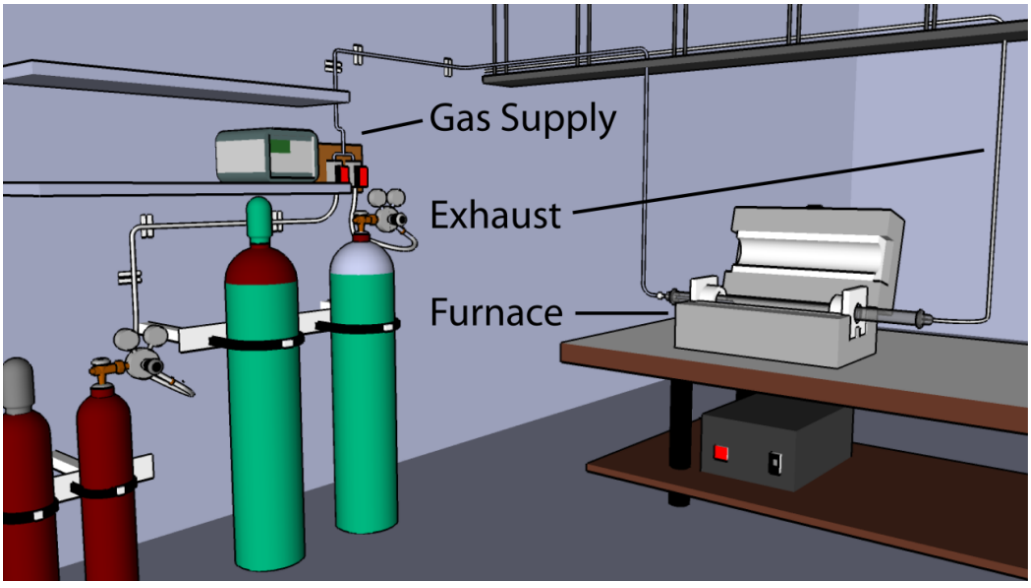

Figure 1: Diagram of thermal-CVD setup

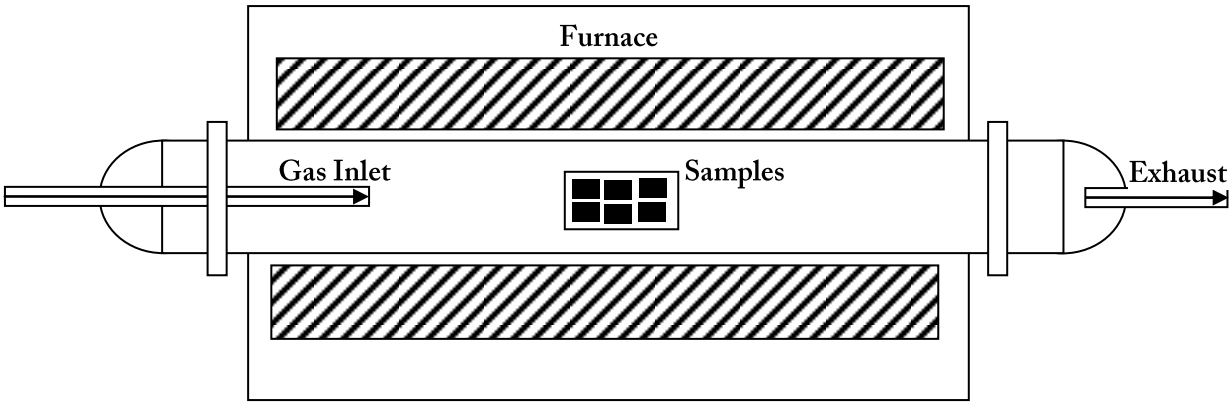

Figure 2: Schematic of CVD furnace showing sample position and gas inlet and exhaust

A schematic of the furnace is shown in Figure 2. The samples were placed, as shown, in the center of the furnace, and the gas inlet tube was placed such that it extended 10-15 cm into the furnace. This length is not precise, because the quartz tube is moved during cleaning, and measurement is difficult.

The CNT synthesis procedure originally developed by Baddour et al. [15] begins with cleaning each stainless steel substrate in acetone for 30 min in an ultrasonic bath. After cleaning, the samples are etched in hydrochloric acid for 5 min and placed inside the CVD furnace. The oxygen inside the quartz tube is purged by injecting nitrogen at 592±5 sccm for 20 min, after which the furnace setpoint schedule program is activated. The temperature controller adjusts the setpoint first from room temperature to 850° C and maintains that temperature for 30 min. Next, the temperature setpoint drops to 700° C, which is the acetylene injection temperature. The carbon source is injected at 45±5 sccm for five min. The furnace is held at 700° C for a further 30 min, then the furnace controller program deactivates, shutting off the heating coils. This procedure was developed for commercial grade multi-purpose type 304 stainless steel strips (w=*0.762 mm*) with mirror finish, but has been adapted successfully for use with type 304 stainless steel meshes by reducing the etching time. The general method is summarized in Figure 3.

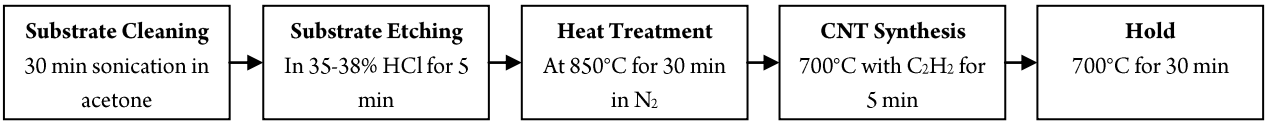

Figure 3: Heat treatment flow diagram

4.2 CVD Experimental Design

To attempt to isolate one parameter that is known to strongly affect steel microstructure, and therefore CNT growth, a series of experiments was designed to investigate the effect of the cooling rate between the heat treatment and CNT synthesis steps of the method in [15]. It was decided that three cooling rates should be investigated, two of which would use an abrupt setpoint change, while the third would use a ramped setpoint change. The first set of experiments, case A, followed the usual method, the second, case B, slowed the cooling rate by placing the stainless steel substrates in a ceramic holder, and the third, case C, slowed the cooling rate further by ramping it down from 850° C to 700° C over 20 min. The heating rate for the third set of experiments was also ramped, to ensure that the substrates were heat treated for only 30 min. Figure 4 shows the temperature setpoint history for each experiment, where the asterisk symbols denote the actual furnace thermocouple reading for cases A & B. For the third set of experiments, the furnace thermocouple did not deviate from the setpoint, so no asterisks are shown.

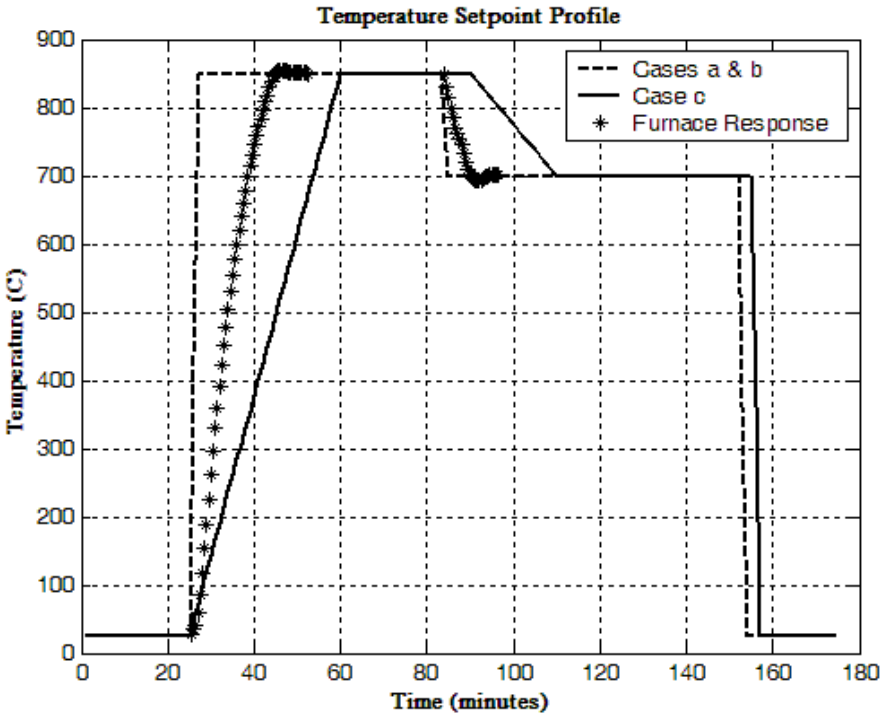

Figure 4: Temperature setpoint plot with actual furnace response

4.3 Sampling and Analysis Techniques for CNT Synthesis

Each of the experiments was repeated four times, and each experiment produced six samples. Substrates used were grade 304SS with mirror finish, with dimensions of 1 cm x 2 cm x 0.762 mm. In addition, the experimental procedure was also done with a set of three uncoated 304SS grids, made for use in a transmission electron microscope (TEM). Samples were analysed using a Hitachi S4700 field emission scanning electron microscope (FESEM) (*5 kV, 10 μA, WD = 7-11 mm*) and a Philips CM200 transmission electron microscope (TEM). The TEM analysis included inner shell ionization x-ray measurement by energy dispersive spectroscopy (EDS), to obtain elemental composition information.

4.4 Dual Plasma Reactor

The plasma chamber used for this project was designed and built by Tavares et al. to produce in flight coated metal nanoparticles [16]. The reactor was originally designed for dual-plasma operation, with a central DC cathode surrounded by four grounded anode bars, in turn surrounded by an RF mesh electrode. The DC electrode is connected to a pulsed DC power supply to generate an electric-arc plasma, while the latter produces a capacitively coupled RF plasma. For this project only the RF plasma was required, so the DC arc plasma assembly was removed. In this configuration, shown in Figure 5, the central electrode is grounded through contact with the vacuum chamber, while the 316 stainless steel mesh acts as the live electrode. CNTs synthesized on grade 304 stainless steel substrates (*100 x 100 wires-per-inch mesh, l = 2 cm w = 1 cm*) using the previously described t-CVD method (case A) were treated in an RF glow discharge of argon and ethane, or argon, ethane, and oxygen. During treatment the CNT samples were placed on a quartz disk, between the two electrodes. Samples were placed at this location, avoiding contact with either of the electrodes to prevent bias from affecting the surface treatment. After treatment the CNT samples were removed from the chamber for analysis and kept in a desiccator to avoid exposure to moisture. Figure 5 shows a photograph of the vacuum chamber and a diagram of the RF plasma electrode assembly that make up the RF plasma system.

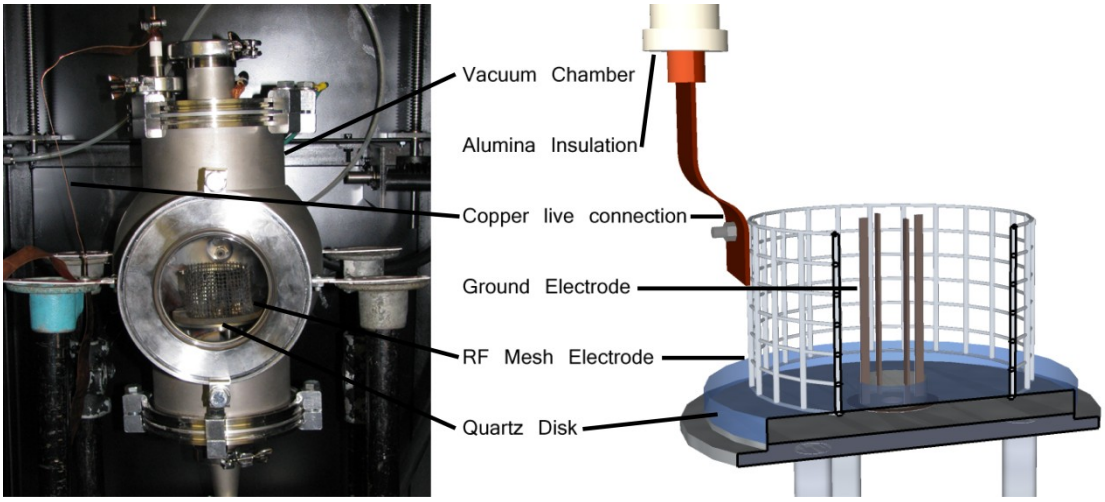

Figure 5: Photograph and diagram of RF plasma chamber system

The plasma chamber consists of a four-way cross manufactured by MDC vacuum products. The chamber is grounded at all times. The RF mesh electrode is made from 316 grade stainless steel and is connected to the RF generator. The quartz disc, manufactured by Technical Glass Products Inc., is used to electrically isolate the wire electrode from the grounded chamber. The central ground electrode is made of four 316 stainless steel bars. The 13.56 MHz RF power is provided by a Dressler CESAR 1312 RF generator, equipped with a VM-1000 A matching network. The RF signal is continuous, and the discharge forms between the live mesh electrode and the central grounded anode bars. The lead connecting the live electrode to the power supply is made of a copper sheet, and is insulated with an alumina sleeve, to prevent the live lead from coupling with the chamber. The entire assembly is placed in a Faraday cage to contain electromagnetic radiation, as shown below in Figure 6.

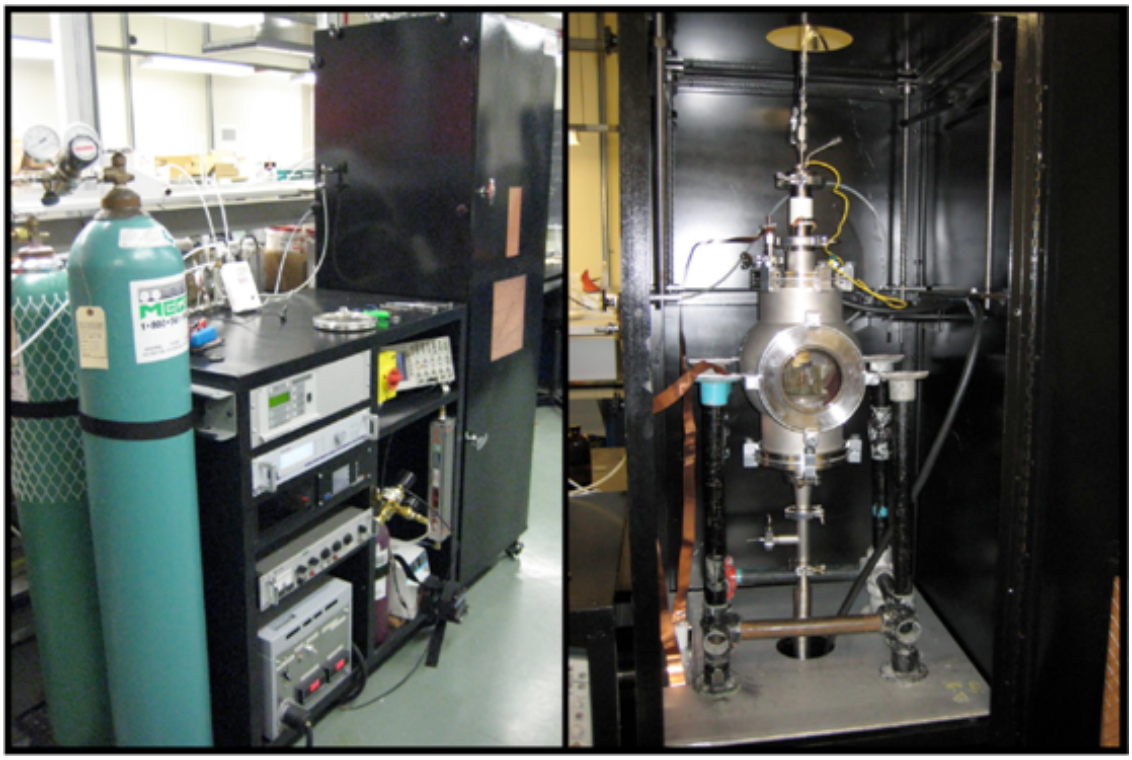

Figure 6: RF plasma reactor setup (Swanson [67])

The experimental procedure begins by evacuating the vacuum chamber to its base pressure of 4 mtorr using a rotary vane Alcatel Pascal 2005 SD vacuum pump. The inert gas used to control the pressure is argon (Ar), while the reactant gases are oxygen (O_2) and ethane (C_2H_6). The flowrate of each of the gases is monitored and controlled using Brooks model 5850E mass flow controllers and a Brooks model 0154 Readout and Control Electronics indicator module. The pressure in the chamber is controlled by a NorCal Intellisys Adaptive Pressure Controller. For all experiments, the flowrate of Ar was maintained at 2000 sccm (standard cubic centimetre per minute), the total chamber pressure at 20 torr, and the load RF plasma power at 20 W. These values were determined in [16] to be optimal for achieving reasonable electrical breakdown voltage , plasma volume and treatment results.

Two different plasma gas compositions were used to produce non-polar (np) and polar (p) surface modifications. These compositions were 2000 sccm Ar and 1 sccm C_2H_6 for np-type treatment, and 2000 sccm Ar, 1 sccm C_2H_6, and 5 sccm O_2 for p-type treatment. These treatment conditions were determind by E. Swanson, and are summarized in Table 1 [67].

For each treatment type, plasma durations of 5, 10, 15, 30, and 60 min were investigated. Two samples were produced in each experiment, and each set of experimental conditions was repeated three times.

Table 1: Plasma gas flowrates [sccm] for non-polar and polar treatments

Gas Flowrate	Non-Polar Treatment [sccm]	Polar Treatment [sccm]
Argon	2000	2000
Ethane	1	1
Oxygen	0	5

4.5 CNT Substrate Analysis Techniques

Prior to the production of nanofluid suspensions, treated CNTs-covered stainless-steel samples were first investigated for observable physical alteration and changes in water interaction properties using the FESEM and the water contact angle goniometer. The Hitachi S4700 FESEM and the Dataphysics model OCA 20 goniometer were used. One sample from each experiment was investigated with the FESEM, and the other with the goniometer. In addition, samples that had been exposed to liquid water were also imaged in the FESEM to check for CNT morphology changes caused by contact with the liquid. The FESEM has already been described, so the remainder of this section will focus on water contact angle measurement.

The goniometer measures the contact angle made between a water droplet and the sample. The measured angle is indicative of the strength of the surface-liquid interaction in the sample relative to the surface tension of the droplet. For example, a sample that is hydrophilic will draw the droplet closer to the surface, maximizing the wetted surface area until surface tension prevents further expansion, giving rise to a small contact angle. With a hydrophobic sample, on the other hand, the sample does not interact strongly with the water, minimizing its contact with the surface and giving rise to a large contact angle [68]. The goniometer operates by first placing the sample on the stage and depositing a 100 μL droplet of reverse-osmosis (RO) water on it. The droplet is photographed using a digital camera while being illuminated from

behind. The silhouette is then traced and the baseline is specified by the user, after which the analysis software calculates the contact angle.

Fourier transform infra-red spectroscopy (FTIR) was used to characterize the surface chemistry of the nanotubes. Infrared spectroscopy devices are fundamentally interferometers, which send one beam of infrared light through a sample and comparing it to a second beam that bypasses the sample. In this way, recording the wavelengths that are absorbed by the sample can reveal detailed information about the chemical groups present [69]. CNTs-covered stainless-steel wire mesh samples were analyzed before and after p-type treatment using standard transmission mode on a TENSOR 27 FT-IR spectrometer with a liquid-nitrogen MCT detector, mounted on a Bruker Optics Hyperion 2000 IR microscope. The objective was a 15x IR lens with a numerical aperture of 0.4. Each spectrum representing one x,y coordinate was recorded for 250 scans. Ambient air was used as the background. The absorption bands were adjusted to fit a baseline using the OPUS v 6.2 mapping software.

P-treated CNTs were removed by shearing onto a carbon-grid for TEM analysis. A carbon-grid is a copper TEM sample grid that is coated with a Vinylec® carbon film on one side. This was done to ascertain the morphology of the coating deposited by the RF plasma treatment, and the chemical composition of the coating by EDS. TEM operating principles have already been described in this chapter, so further description is omitted.

4.6 Nanofluid Sample Preparation and Analysis Techniques

To prepare aqueous suspensions of CNTs, wire mesh samples (*100 x 100 wires-per-inch mesh, l = 2 cm w = 1 cm*) that had been treated using the t-CVD case A procedure and exposed for 15 min to p-type RF treatment were sonicated in 2 dram (*7.4 ml)* vials for 5 min in 5 ml of RO water. The suspensions were analyzed using UV-VIS absorption spectrometry, ζ-potential measurement, and visual (digital camera) inspection. To test for thermal stability, aqueous CNT suspensions were boiled for 20 min and re-analyzed. For UV-VIS absorption measurement, the suspensions were diluted 2:3 with RO water. For ζ-potential measurements, a dilution ratio of 1:3 was used. Dilution was necessary to prevent saturation and fouling of the detectors.

UV-VIS absorption spectrometry is a technique whereby light with wavelengths between 200 nm and 800 nm is passed through a quartz cuvette containing a liquid sample. The visible and ultraviolet photons are absorbed or transmitted by the sample, and a detector records a spectrum of transmitted intensity vs wavelength. In the case of a nanofluids, the nanoparticles or CNTs suspended in a liquid absorb the ultraviolet light, resulting in a characteristic wide absorption peak in the UV range [70]. Since CNTs appear black under white light illumination, a CNT nanofluid is expected to absorb broadly across the visible range. The UV-VIS absorption spectrometer uses 1 cm^2 x 3 cm (3 ml) quartz cuvettes and a minimum liquid volume of 2 mL. The instrument used for this project was a model 8453 UV-VIS spectrometer, manufactured by Agilent, USA.

ζ-potential measurement is a method for determining the stability of a suspension. The sample volume used was 900 μL. The measurement device, a Malvern Instruments Nano Z-sizer ZS90, detects the mobility of suspended particles by measuring their movement in response to an electric field that is applied in the fluid. This applied field is correlated to the surface charges of the suspended particles, and is recorded as the suspension ζ-potential [mV]. The relationship between suspension stability and ζ-potential arises from the mutual repulsion that occurs between like-charged particles. For this reason, particles with a strong surface charge tend not to agglomerate, since contact is opposed. Typically accepted ζ-potential values are summarized below in Table 2. In general, a suspension with a measured ζ-potential above 30 mV (absolute value) is considered to have good stability [71, 72].

Table 2: ζ-potential and associated suspension stability

ζ-potential (*absolute value [mV]*)	**Stability**
0	Little or no stability
15	Some stability but settling likely
30	Moderate stability
45	Good stability, possible settling
60	Very good stability, little settling likely

Ethanol suspensions were also prepared for use in the SEM and TEM to ascertain whether nanofluids were composed of CNTs removed during sonication and, if so, whether the CNTs had agglomerated while in suspension. Ethanol suspensions were prepared by sonication of 1cm x 2cm p-treated CNTs-covered mesh samples in 5 ml of ethanol for 10 min in a 2 dram vial. Afterwards, the suspension was sampled and deposited drop wise onto a carbon grid. The carbon grid was left to dry in a fume hood for 3 hours, and then taken to the SEM. After SEM analysis the grid was stored in a desiccated chamber until TEM analysis.

5. Results and Discussion

5.1 Effect of Heat Treatment on CNT Growth

The main goal of the heat treatment study was to assess if the cooling rate, and not just the temperature setpoints, had an effect on the growth of CNTs. There has not yet been established a mechanistic connection between the grain structure of stainless steel and the growth of CNTs, but it is surmised that the former influences the latter. Figure 7 shows a series of SEM micrographs taken from representative samples produced by the three heating protocols described previously. The changes in CNT growth morphology and density of the CNT layer are dramatic. In Fig. 7A, corresponding to heat treatment case A, CNTs are seen to be in a low density layer, with little to no alignment. Heat treatment case B, shown in Fig. 7B, where the cooling rate was retarded by placing the samples in a ceramic holder, showed a much denser CNT layer with a high degree of alignment. CNTs in these samples were shorter relative to those from case A. Case C, in Fig 7C, failed to produce any CNTs, yielding only amorphous carbon. Although this does not prove that a link between surface structure and CNT morphology exists, it does provide strong circumstantial evidence in that regard, and demonstrates that although temperatures are important, the cooling rates are as well.

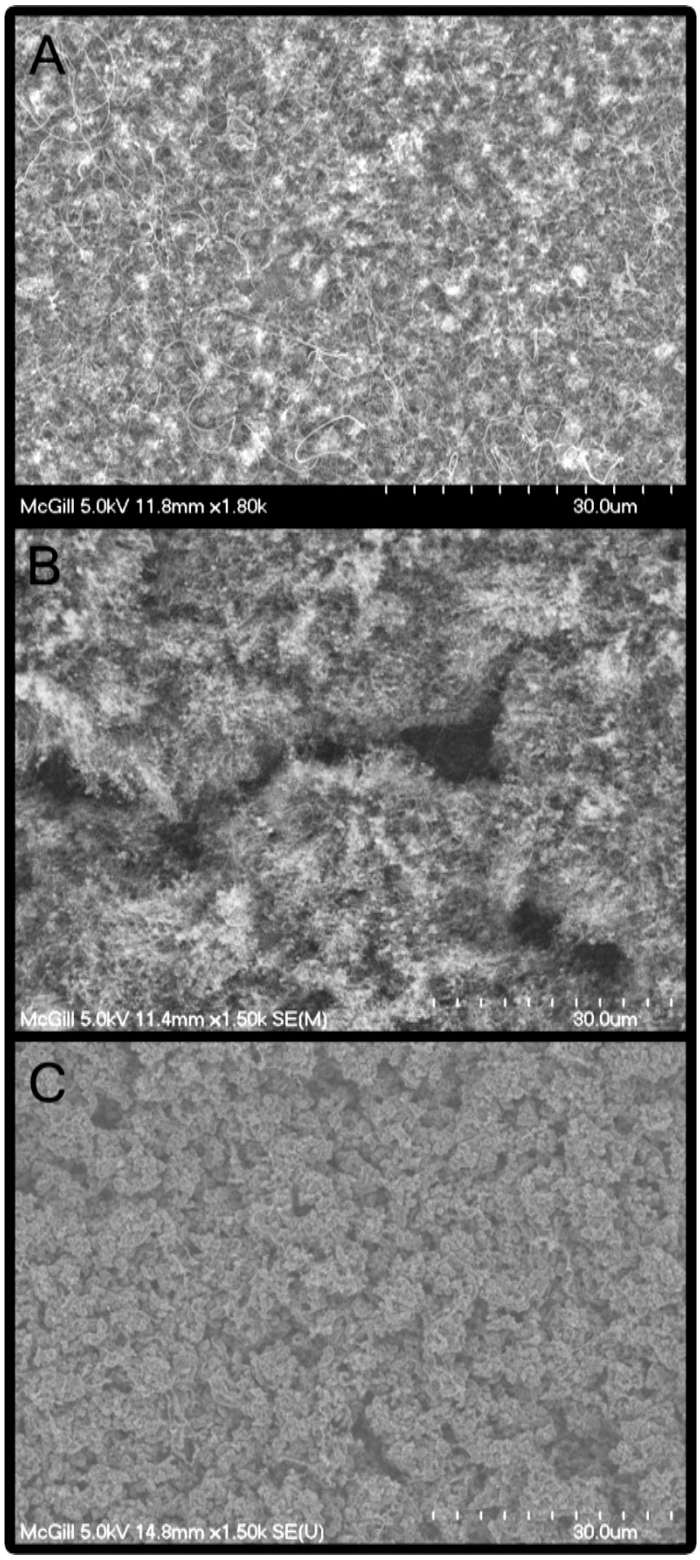

Figure 7: CNT morphologies for cases A, B, and C

To determine if the cooling rate indeed affected the surface microstructure of the stainless steel, samples were etched in HCl for five min and treated according to cases A and B, but without injection of acetylene. The resulting SEM micrographs are given in Figure 8. From these images, it is clear that the different cooling rates resulted in different surface microstructures. Along what appear to be grain boundaries, the two heat treatments produced different surface phases. Treatment B, in Fig. 8B, shows a visible crystallite network, evidenced by saturation of the SEM image, that is absent from the Case A sample. Grain size analysis revealed that the grains have the same average size in both treatments, approximately 5-15μm. This is not surprising, because grain size variations are not expected for slight deviations in the heat treatment. The different shaded regions in Fig. 8A correspond to regions of different surface crystal deposits, which appear at first like grains, but closer inspection of the samples revealed many grain boundaries within the dark regions. Higher magnification images, shown in Fig. 9A and Fig. 9B, further illustrate the differences in surface structure resulting from the two heat treatments. These images both focus on regions that seem to be surface grain boundaries. With the Case A treatments, the surface is covered with spiny plate-like crystals, while with Case B treated samples the crystals covering the surface are smaller, more uniformly sized, and a second type of crystal is seen to have formed in the grain boundaries. X-ray energy dispersive analysis (EDS) of these samples with the FESEM was inconclusive due to interaction volume limitations on the maximum spatial resolution, but it is likely that the crystal phases are compounds of chromium, carbon, and iron, as seen in the EDS using the TEM, described later.

The significance of the different surface structures with respect to CNT growth is unclear from these images, as is the physical cause of the differences, but the effect of heat treatment on surface structure is important, because it links the stainless steel surface morphology to observed CNT growth morphology.

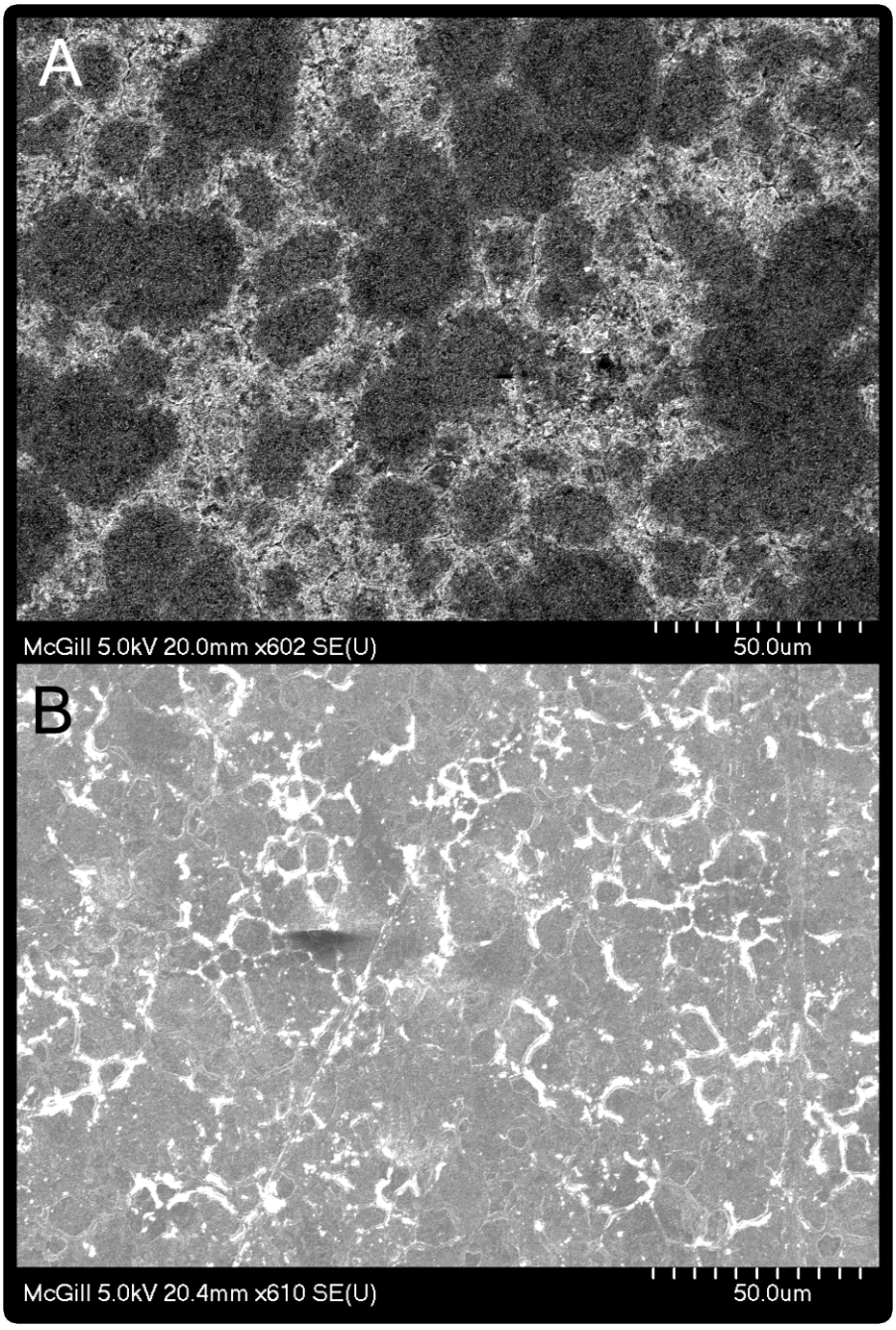

Figure 8: Surface structures for cases A and B from experiments without C_2H_2 injection

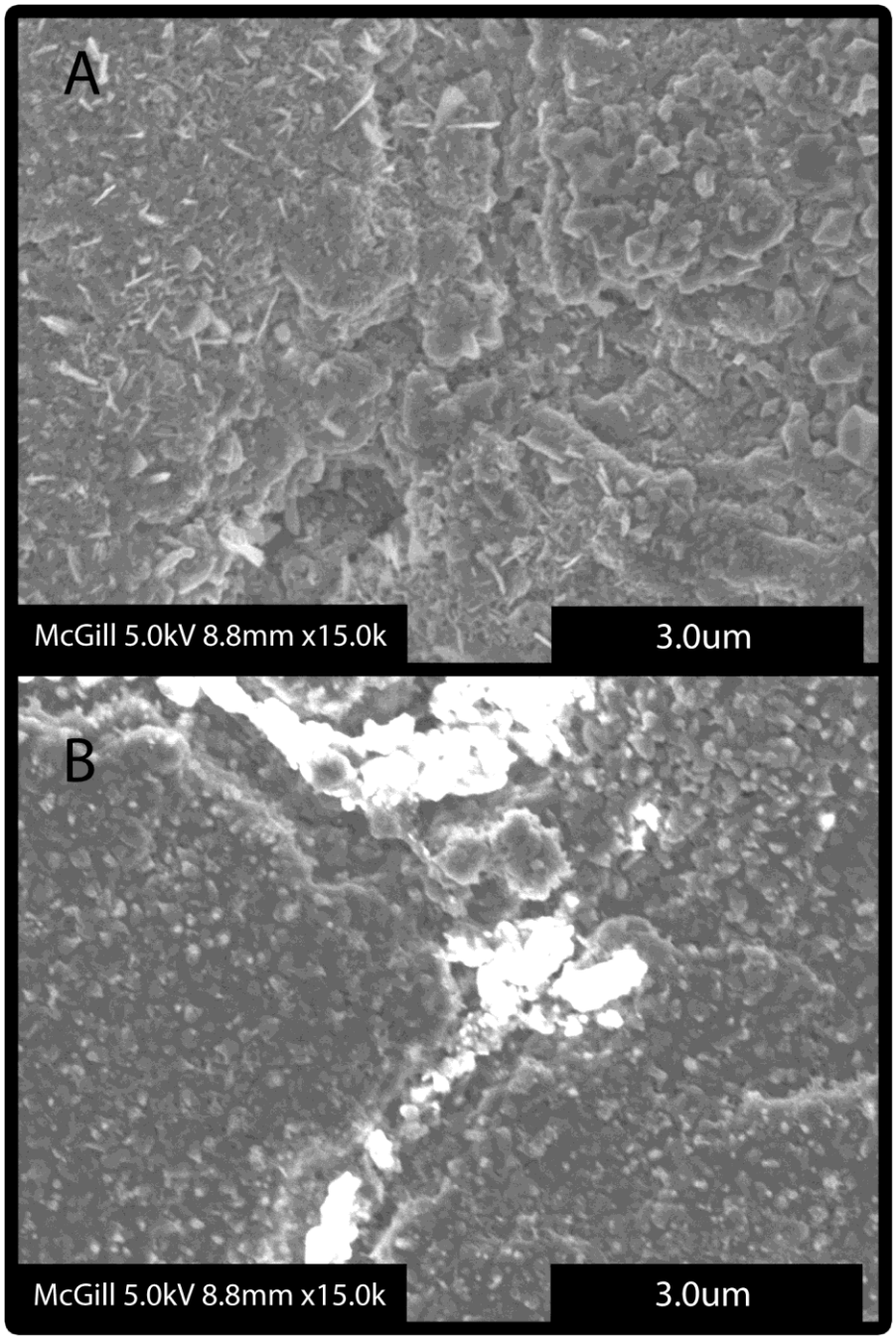

Figure 9: Higher Magnification Images of Surface Microstructures for cases A and B. Case A microstructure includes plate-like crystals, while case B does not. case B has a second type of crystal precipitated at the grain boundaries

Further evidence for the influence of cooling rate on CNT growth was found by examining the undersides of samples produced in experiments testing heating case B, those that had been placed in a ceramic holder. SEM micrographs were taken of the undersides of several samples according to Figure 10, which shows a diagram of one sample with labels indicating regions where the micrographs were taken.

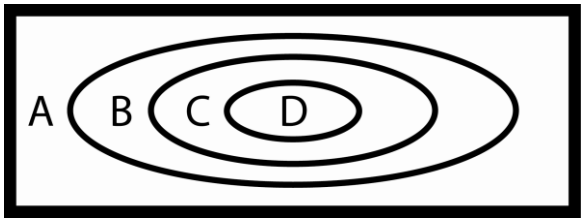

Figure 10: Diagram showing regions corresponding to micrographs in Fig. 11 and Fig. 12

The micrographs in Figure 11 show that CNT growth morphology changed with position on the sample surface. Each region is shown at low and high magnifications. In region A, CNTs grew in aligned and high density bundles, separated by low density growth. In effect, CNT growth in region A resembled a combination of the types previously observed in cases A and B in Fig. 7. In region B, CNT growth was uniformly dense and aligned, as was seen in case B. In region C, CNT growth seemed to be confined to patterns resembling grain boundaries. This was a growth type that had not been observed previously, and offers further evidence for a link between surface structure and CNT growth.

The first direct evidence of a relationship between surface structure and CNT growth was found in region D of Figure 10. In SEM micrographs given in Figure 12, grain boundaries are visible, and a relationship between grain boundaries and CNT growth is immediately apparent. In both micrographs, high density CNT bundles are seen being confined within individual grains on the surfaces of stainless steel samples. Furthermore, it appears that there is a consistent gap between the grain boundaries and the CNT bundles. This observation supports that of Fig. 11C, where CNTs appeared to be growing preferentially in the same shape as grain boundaries. In Fig. 12A, however, the bundle is visibly hollow. It seems that some of the bundles are annular, and not filled as is seen in Fig. 11A. In another image taken of the CNTs in region B of Fig 10 at a tilt angle of 10°, shown in Figure 13, a pattern of taller

CNTs is seen protruding from among the shorter CNTs that matches the patterns seen in region C. Although the CNT growth density is uniform, the lengths of the CNTs are not. This further indicates that CNTs grow first in a region that is at a certain distance from the grain boundary, but within a specific band that does not extend to the center of the grains.

The best explanation for the position dependence of CNT growth is that the inner regions of the samples cooled slower than the outer regions, leading to a variable surface structure. Carbon concentration profiles also undoubtedly affected CNT growth on the undersides of the samples, considering the mass-transfer limitation of carbon vapour reaching the inner regions of the sample underside. For regions A, B, and C in Fig. 8, however, the CNT coverage was nearly complete, and the growth density was higher in region B than in region A, so it does not seem that carbon depletion had as significant an effect on CNT growth as surface structure until region D.

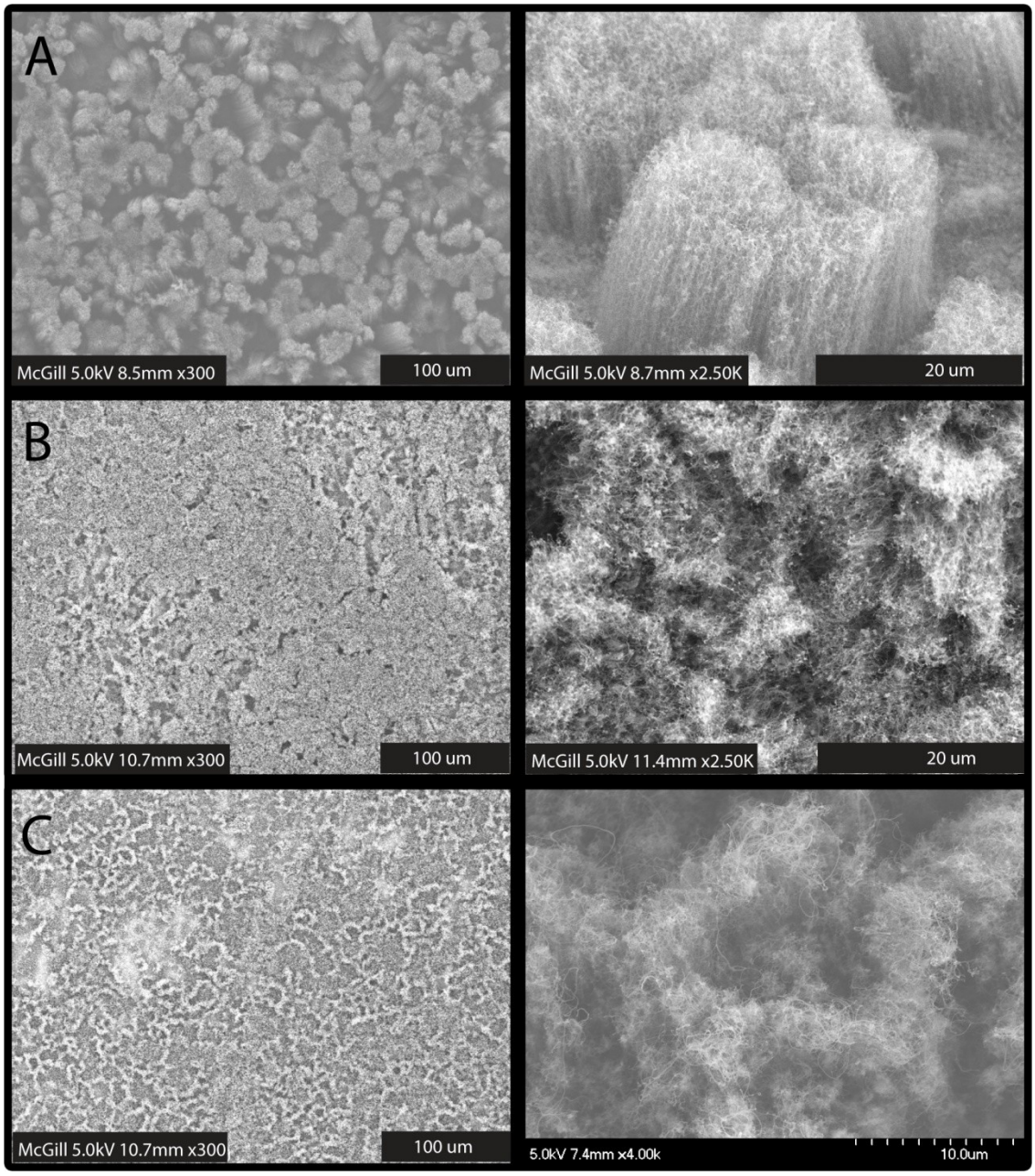

Figure 11: Position dependent growth of CNTs for regions A, B, and C defined in Fig. 10. Left : column x300 mag. Right: x2.5k and x4k mag.

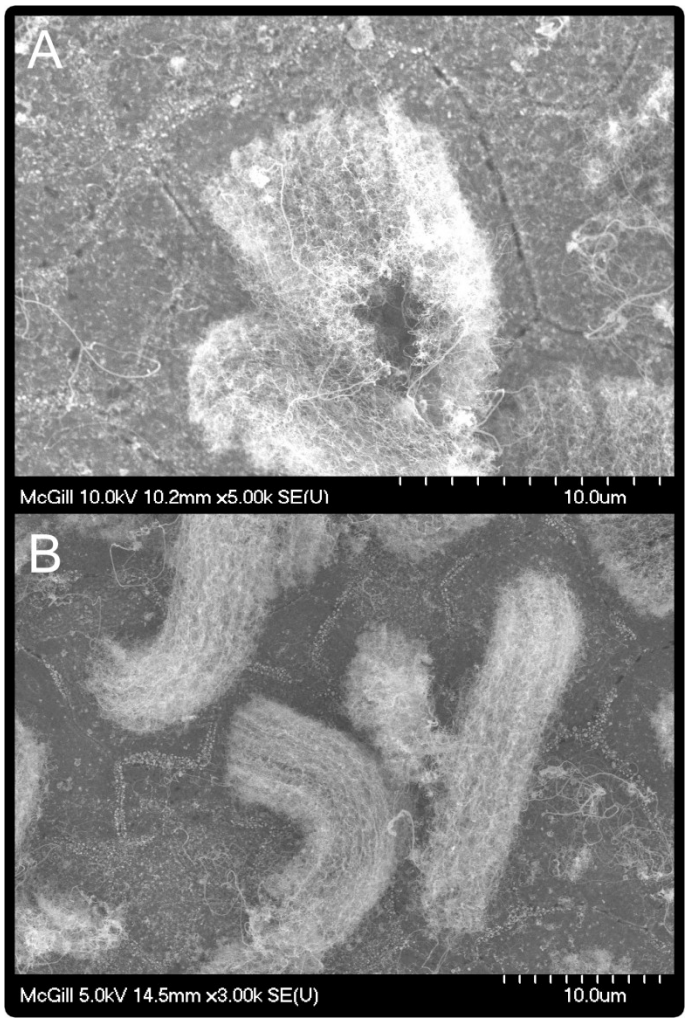

Figure 12: Bundled CNT growth in region D of Fig. 10

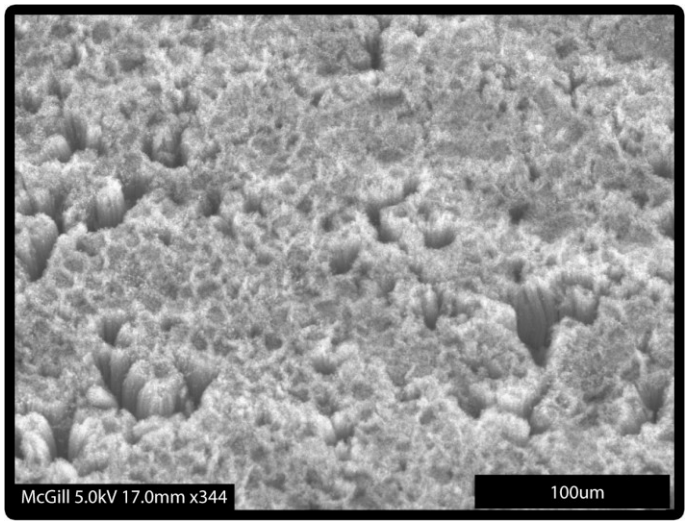

Figure 13: Bundled CNTs from region B showing raised pattern matching Fig. 11C

From a review of the literature, several possible reasons can be identified for CNT growth to be confined to specific regions relative to the grain boundaries. These mostly have to do with the surface composition of the steel, and diffusion of chromium to the grain boundaries during heat treatment in a phenomenon known as *sensitization* [35]. It is not the purpose of this master's project to determine the role of surface chromium concentration on CNT growth, so no conclusions will be drawn. There is evidence, however, that indicates the importance of the development of surface metal phases for CNT growth, and the influence of surface morphology on CNT morphology. Figure 14 shows an SEM micrograph taken from region D, revealing two morphologies of surface crystals. Along the grain boundaries are seen large white crystals, and grown on the surface of one of the grains is a second morphology of small plate like crystals. The region with the smaller crystals is seen to have a sparse coverage of CNTs, distributed uniformly across it. On the other hand, adjacent grains do not show any CNT growth, similar to what was seen in regions where the first crystal morphology dominated, as in Fig. 12B. This seems to show a link between surface morphology, grain size, or grain orientation and CNT morphology, but the chemical composition of the crystals cannot be found using the FESEM. For high spatial resolution information a TEM is required. For this reason, three SS304 TEM grids were subjected to treatment according to case B, and analyzed in the TEM for compositional information. Two TEM micrographs are shown in Figure 15. Corresponding to images A and B in Fig. 15 are two EDS spectra shown in Figure 16. The compositions, recorded in quantitative mode, of the regions probed by EDS are given in Table 3. It was found that the small plate like crystals, shown in Fig 15A, were approximately 47 at% Cr and 53 at% Fe, which is far higher than the relative amount of Cr in SS304, at 18% Cr [33]. Furthermore, Fig 15B shows a region where tubes were present, and the composition of the surface was only 36 at% Cr and 63 at% Fe.

Table 3: X-ray composition information from Fig. 15

TEM Image	Cr composition	Fe composition
304-Grade Stainless Steel	18% (atomic percent)	71% (atomic percent)
Fig 15A	47% (atomic percent)	53% (atomic percent)
Fig 15B	36% (atomic percent)	64% (atomic percent)

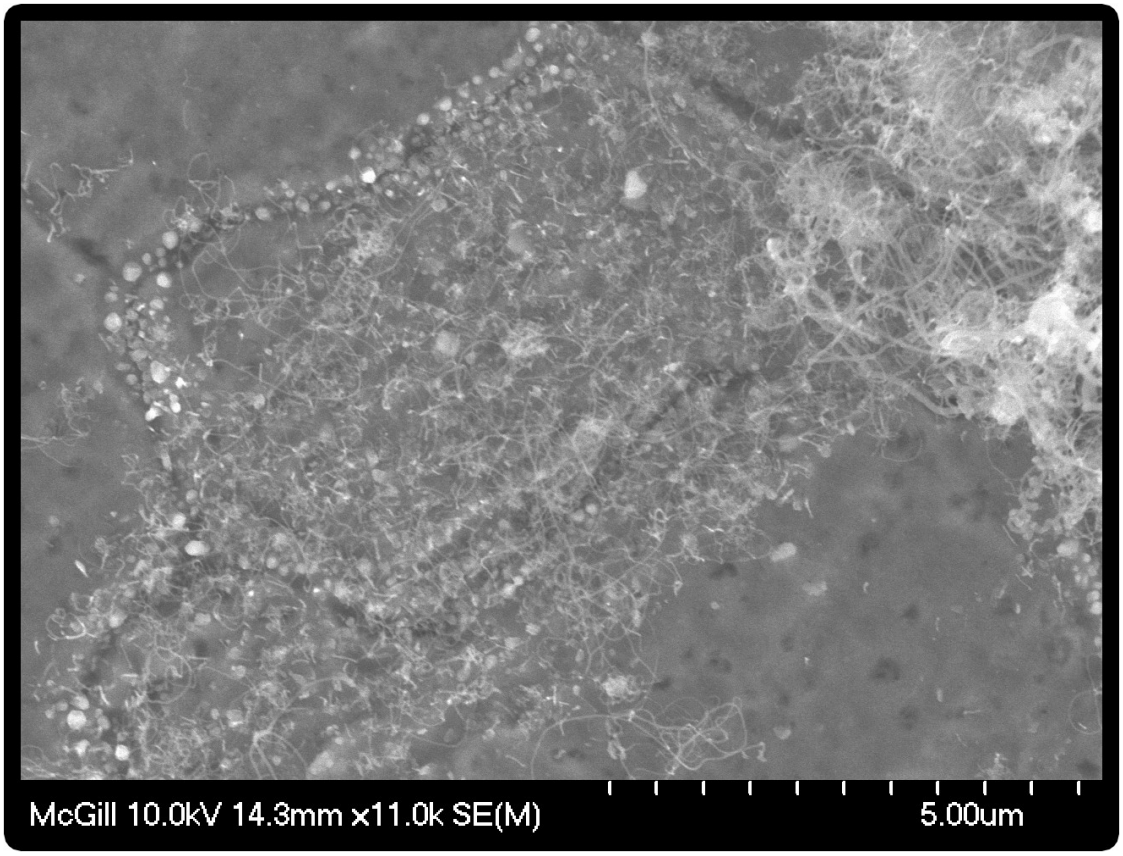

Figure 14: Magnified region showing two crystal morphologies and the effect on CNT growth. Large white crystals grow along grain boundaries, while small crystals cover the surface of the grain in the center of the image. CNTs are visible in the region with small crystals.

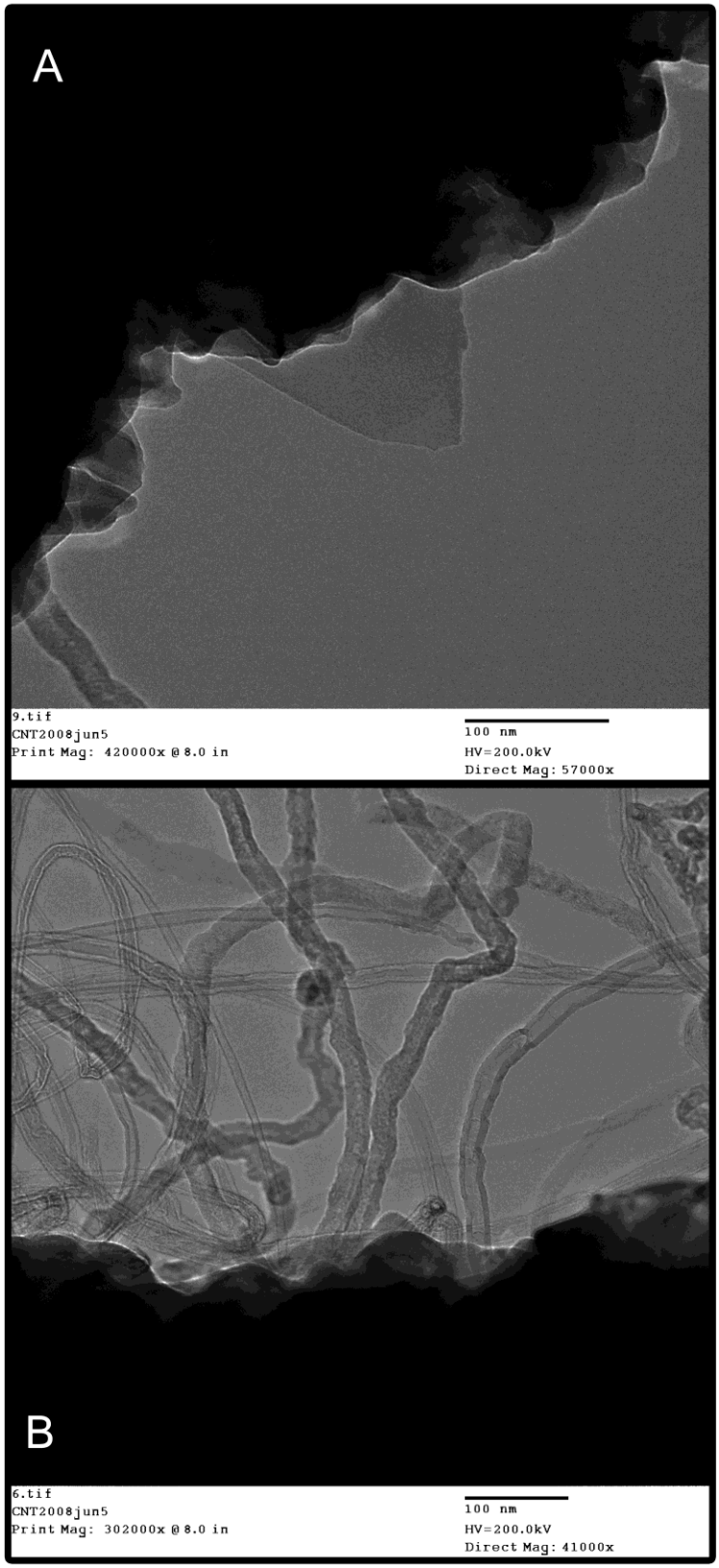

Figure 15: 304 SS TEM grid prepared by case B. A: Surface crystal B: Region with CNT growth

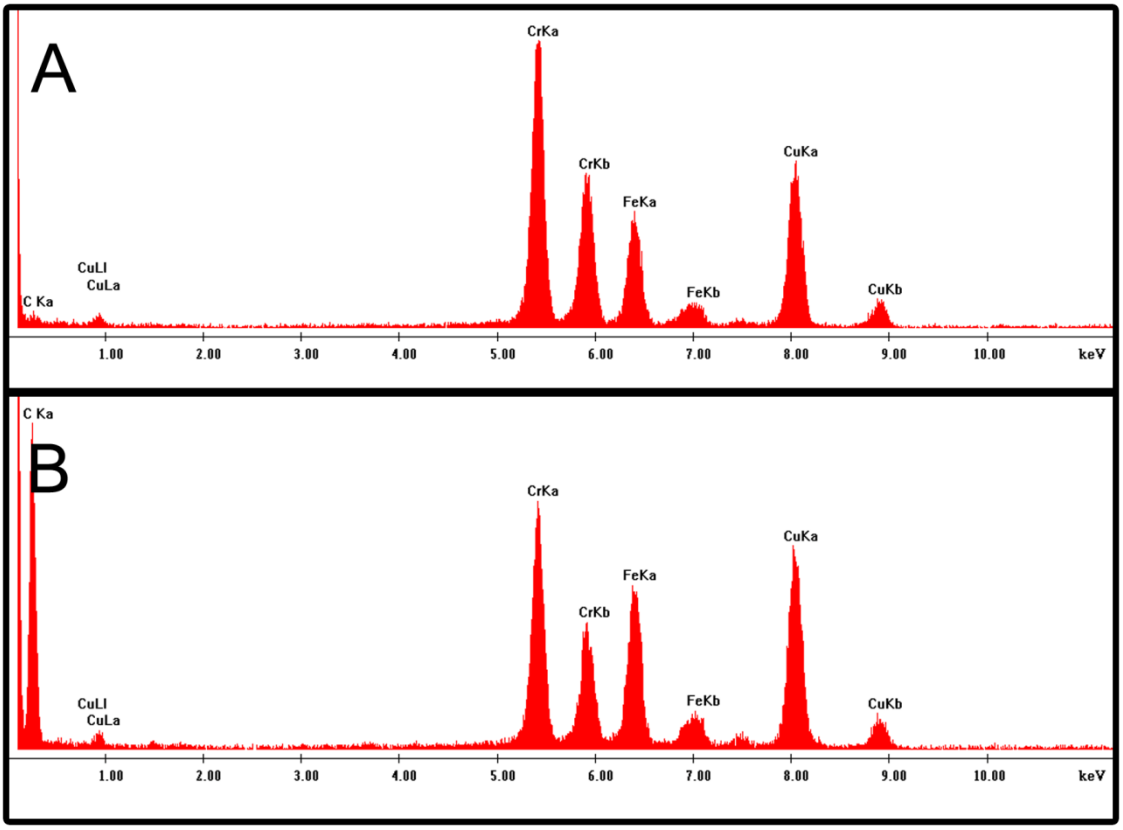

Figure 16: EDS spectra corresponding to Fig. 15 A: Single crystal spectrum, B: Surface spectrum

It is impossible to tell from this evidence if the crystal in Fig. 15A is similar to those seen in Fig. 9 or Fig. 14, but its composition makes it a likely explanation. Some articles, discussed in the literature review chapter, describe that during heating, the chromium present in stainless steel tends to migrate to the grain boundaries or to the surface, and to precipitate into crystalline carbide phases [35, 36]. This leads to depletion of chromium in a zone around each precipitated carbide crystal. There is further support in the literature for the influence of cooling rate from 850°C to 700°C on carbide precipitation, stating that slower cooling rates lead to the formation of more uniformly distributed carbide nuclei [34-36]. It would seem that within the gap where no CNTs grew, Cr was mobile enough during the heat treatment time to migrate to the grain boundaries, leaving a region of exposed iron and carbon. Past the gap, Cr precipitated into nuclei that did not migrate. This sort of diffusion behaviour could conceivably create numerous small sites of exposed iron or nickel, acting as catalyst sites for CNT growth. In conjunction with this, the research showing the effect of iron particle

diameter on CNT growth in studies with deposited iron catalyst particles [73-75] could help explain why CNTs were seen to only grow a certain distance away from the grain boundaries. It seems that within the zone where CNTs are seen to grow, the exposed iron sites are of the ideal size and that the carbon concentrations are sufficient for high density CNT growth. Unfortunately, this evidence alone cannot prove that carbides are responsible for CNT growth or morphology, but it does make a strong case for further investigation.

EDS analysis was attempted to map the metal concentrations within individual grains, but again the interaction volume of the electron beam precluded the collection of such surface specific information.

5.2 Analysis of CNTs on Stainless Steel Substrates

The first analysis of treated CNTs-covered mesh samples was for bulk water contact angle. One sample from each experiment was tested for response to a 100 μL droplet of RO water. The three types of samples tested were untreated, np-treated, and p-treated. The average contact angle for the control samples was 103.4° (*s.d.* = 9.5°). For all np-type CNTs-covered mesh samples, the repulsion from the surface was so strong that the droplet would not adhere to the surface. This prevented any contact angle measurements from being recorded. For all p-type CNTs-covered mesh samples, on the other hand, the water droplet completely wetted the surface. This again prevented any contact angle measurements from being recorded. Both sample types were tested two weeks after treatment, and no change in water interaction properties was observed. Figure 17 shows three images of CNTs-covered mesh samples obtained using the goniometer camera. Fig. 17A shows a control sample; Fig. 17B shows an np-treated sample; Fig. 17C shows a p-treated sample.

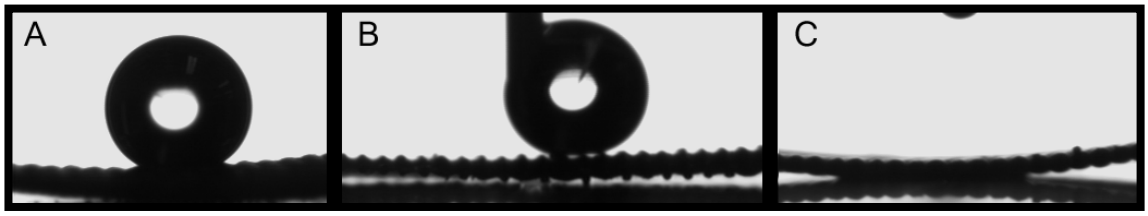

Figure 17: Water contact angle measurements. A: Untreated CNT sample B: np-treated CNT sample C: p-treated CNT sample

These dramatic changes in water interaction show that the plasma treatment was modifying the surfaces of the samples, but water contact angle measurements could not reveal whether the surfaces of the CNTs themselves were being modified, or if the result arose from modification of the steel, or even by removal of the CNTs. To investigate potential changes of the CNT surface, SEM and FTIR analyses were used to gather morphological and chemical information, respectively.

Examination of np-type CNTs with the SEM clearly revealed that a plasma polymer layer was being deposited during the RF plasma treatment. Furthermore, the SEM observation showed that the layer is electrically insulating, uniform, and increases in thickness with increasing treatment duration. As the thickness of the deposited layer grew, the decreasing conductivity of the samples led to charging effects in the SEM. Figure 18 shows a set of three images depicting the change in surface charging for five (A), ten (B), and thirty min treatments (C).

Figure 19 shows a set of twelve images, summarizing the morphological differences of the surface coating resulting from 5, 10, 30, and 60 min of RF plasma treatment (rows) taken at x5k, x20k, and x60k magnification (columns). The images show that with increasing treatment time, the CNT surfaces become increasingly electrically insulating. At x60k magnification, it is further seen that the individual coated CNTs start to join (3,3). Although the surface coating was not yet visible and did not cause charging effects after 5 min of np-treatment, the samples fully repulsed water droplets and did not lose their effectiveness after two weeks. This observation indicates that a hydrophobic CNTs-covered mesh surface can be produced that retains its electrical conductivity. Considering that the CNTs grown by t-CVD are electrically coupled to the metal substrate beneath them [19, 32], this new material presents a promising option for future development of chemically protected sensors that can be safely inserted into an aggressive environment.

The most dramatic effects of np-treatment were seen in samples treated for 1 hour. Figure 20 shows four more SEM images of np-treated CNTs-covered mesh samples. In these particular samples, two types of deposited layer were found: individually coated CNTs, and a plasma

polymer layer in which CNTs were embedded. Images (4,1) through (4,3) of Figure 19 demonstrate this type of layer. The solid layer is especially interesting, because it shows that a polymer-CNT composite can be produced without any of the wet chemical functionalization or difficult blending steps that are currently required [76].

The SEM study clearly showed that the np-type RF plasma treatment coats each tube individually, and that the thickness of the deposited layer can be controlled by selecting an appropriate treatment time.

An FTIR analysis of the np-type coating produced by RF treatment, with the same gas compositions and operating conditions, has been reported by Tavares et al. [16]. The analysis indicated that the plasma polymer coating consisted of saturated hydrocarbons with a low degree of polymerization, but a high degree of cross-linking. A TEM analysis of coated nanoparticles showed that the RF plasma treatment deposited a layer of uniform thickness around copper nanoparticles.

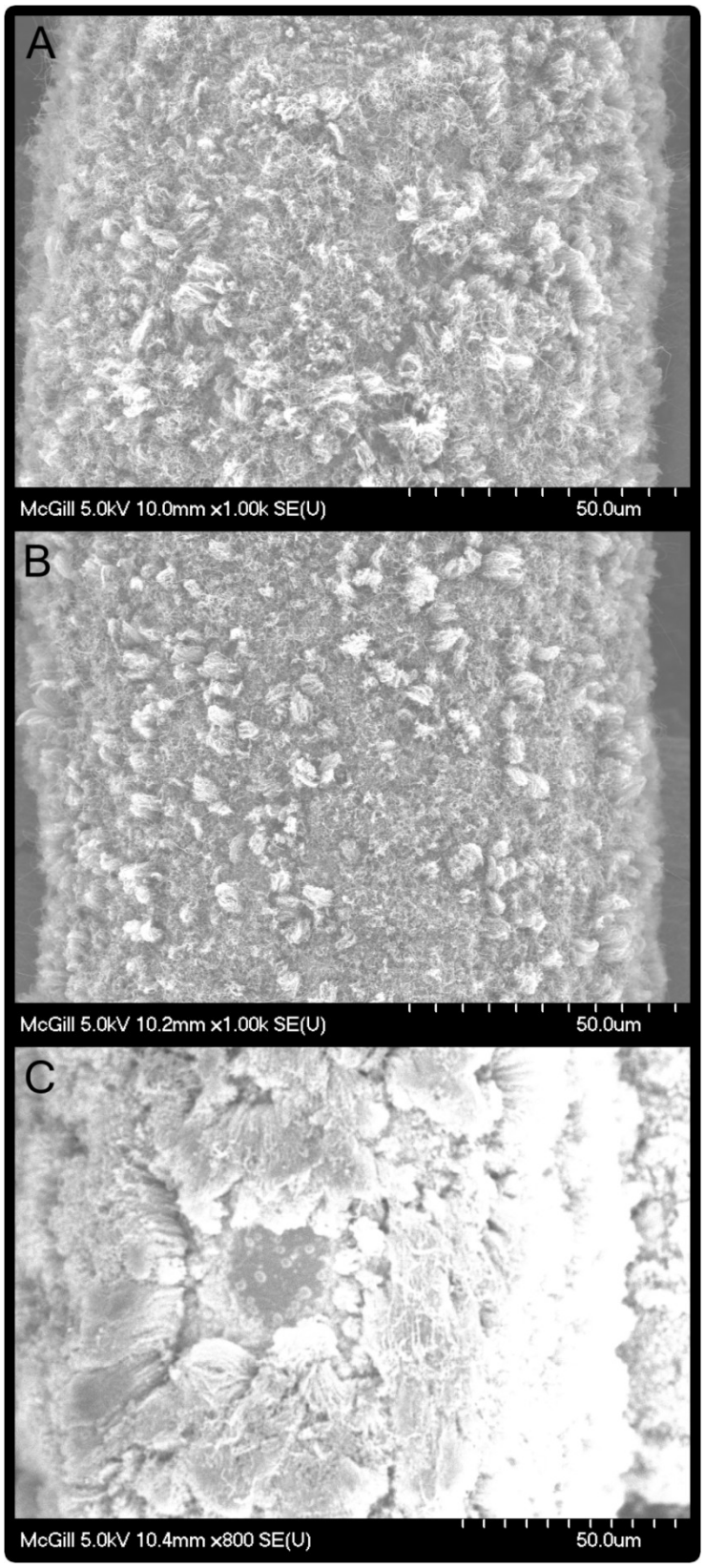

Figure 18: Development of np-plasma polymer and associated charging effects on SS304 mesh samples. A: 5 min np-treatment B: 10 min np-treatment C: 30 min np-treament

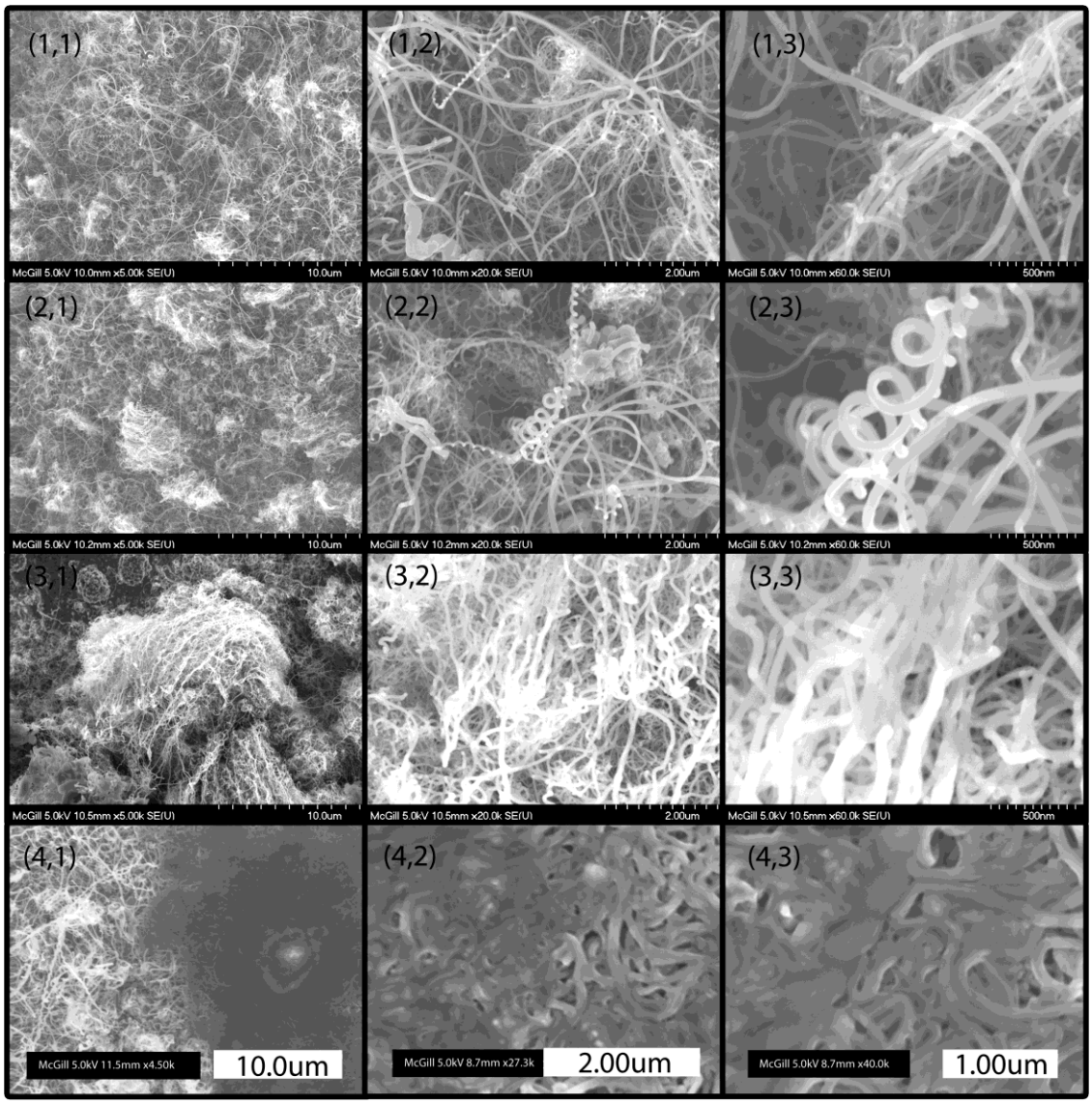

Figure 19: FESEM micrograph array of the development of a plasma polymer layer after np-type RF plasma treatment. Columns show increasing magnification. Column 1: x5k, Column 2: x20k, Column 3: x60k. Rows show increasing treatment time. Row 1: 5 min, Row 2: 10 min, Row 3: 30 min, Row 4: 60 min

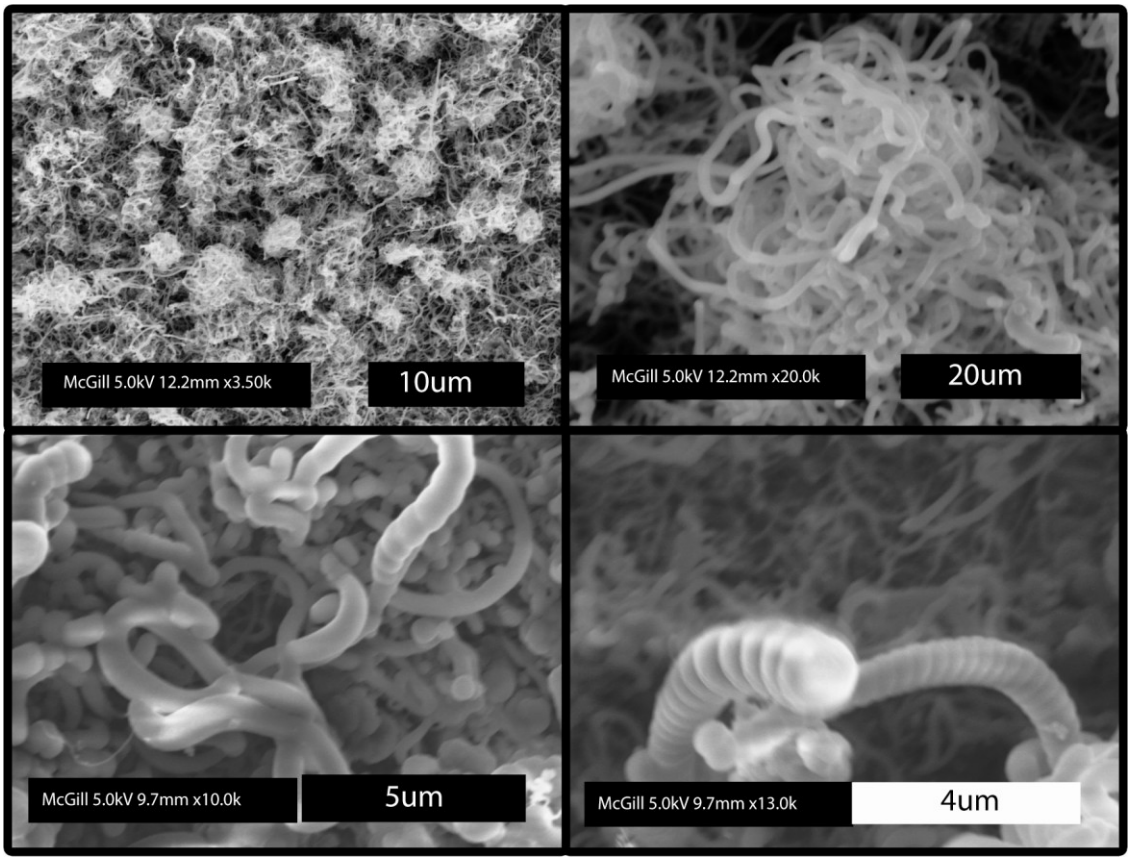

Figure 20: 60 min np-treatment of CNTs-covered mesh samples

P-treated CNTs-covered mesh samples analyzed in the SEM did not at first give any visual indication of being affected by the p-type treatment. Unlike np-type CNTs, the p-type did not develop a visible coating, and did not show any dramatic change in morphology. The only noticeable change was that for treatment times of 30 min or more, the CNTs were removed from the substrate, leaving a clean surface. From this it was surmised that the p-type treatment was not actually depositing a layer, but rather was modifying the surface chemistry of the CNTs by opening the outer walls and attaching polar surface groups. In this way, the disappearance of the CNTs from the surface after prolonged treatment could be explained as a gradual degradation of the graphene structure, ending in complete oxidation. This was verified by TEM and FTIR analyses, which are discussed later in this section. Investigating the p-type samples that had already been exposed to liquid water, however, revealed a significant change in CNT morphology. CNTs, grown in non-contiguous bundles, had changed their morphology to maximize contact area with each other. Because the samples had displayed very strong hydrophilic properties, it was concluded that this change occurred during drying, as a result of the natural tendency to maximize surface area exposed to water. Figures 21 and 22 show p-type CNTs before and after exposure to RO water, for treatment times of 15 min and 10 min, respectively. In Fig. 21, the left column (A, C and E) shows CNTs that had not been exposed to RO water; the right column (B, D, and F) shows CNTs after exposure to RO water. This clear attraction to polar liquids on the part of the p-type CNTs demonstrates that the RF plasma treatment affected each tube surface. The curling of the tube tips that is visible in Fig. 22B is indicative of the introduction of defects into the graphene structure of the CNTs [11], which furthers the hypothesis that the p-treatment is altering the chemical structure of the CNTs rather than depositing an external layer.

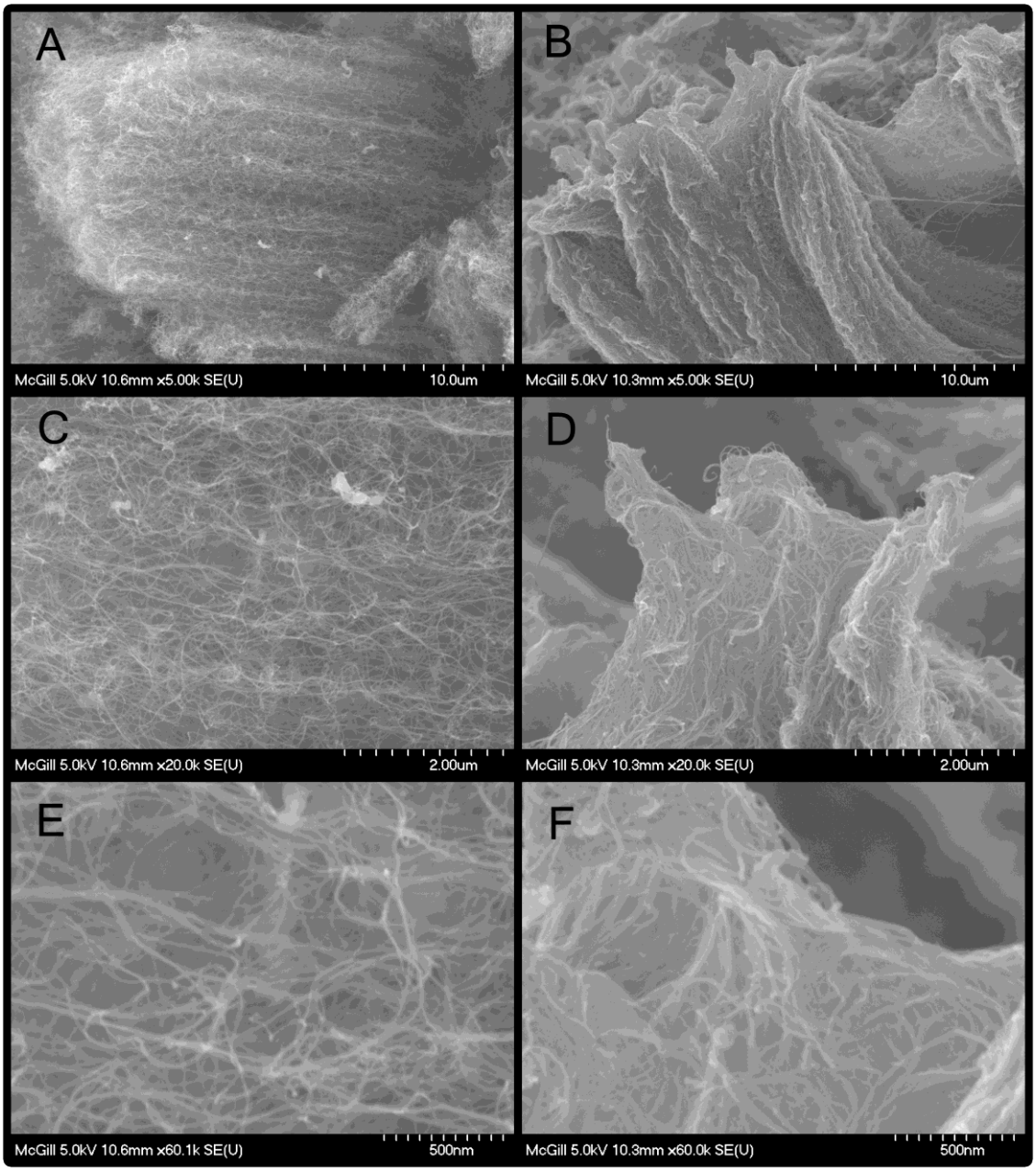

Figure 21: 15 min p-treatment of CNTs before (A, C, and E) and after (B, D, and F) contact with RO water. A: x5k, B: x5k, C: x20k, D: x20k, E: x60k, F: x60k

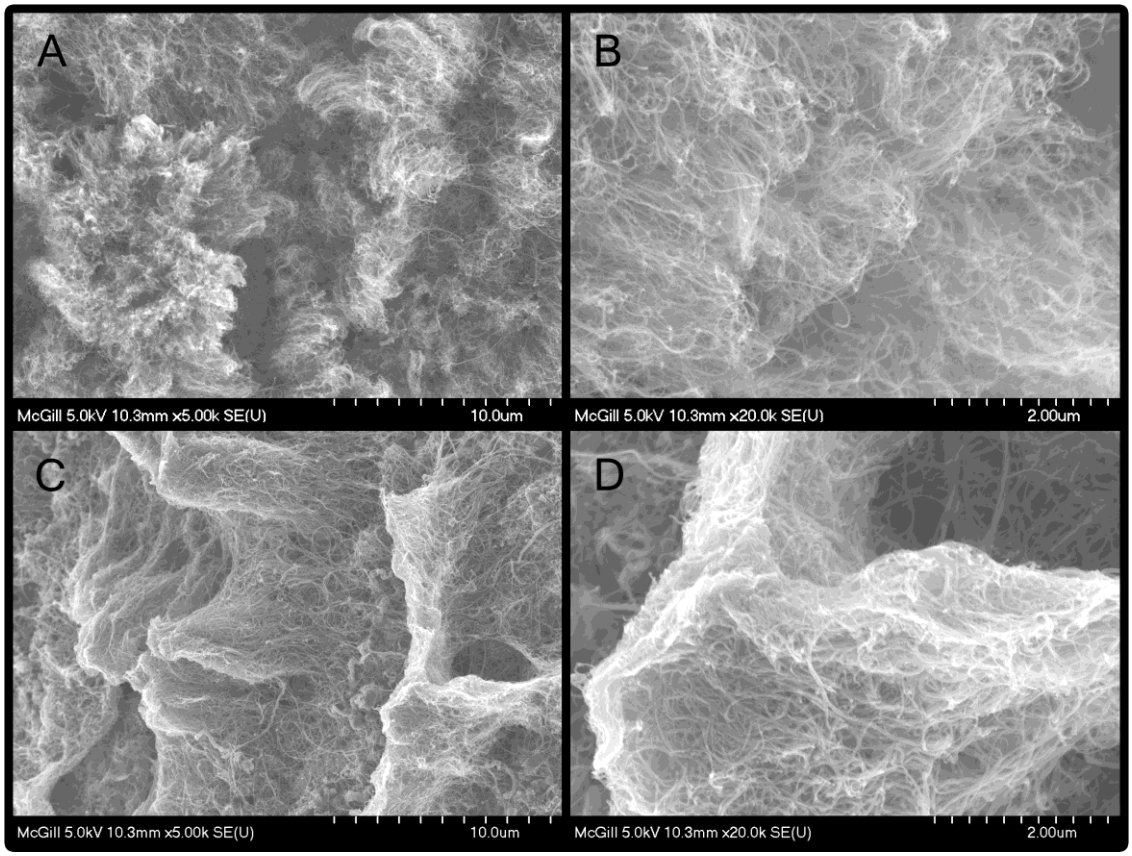

Figure 22: 10 min p-treatment of CNTs before (A, B) and after (C, D) contact with RO water. A: dry CNTs x5k, B: dry CNTs x20k, C: wet CNTs x5k, D: wet CNTs x20k

The SEM analysis, despite revealing the strong hydrophilicity of individual CNTs, could not demonstrate whether the p-treatment actually deposited a plasma polymer layer. To examine the CNTs surface with sufficient resolution, a carbon-grid was prepared for use in the Philips CM200 TEM. Two images collected with the TEM of p-type samples treated for 15 min, corresponding to the strong hydrophilic response seen in Figure 21, are shown in Figure 23. These images definitively show that no plasma polymer layer is deposited, but rather that the outer walls of the CNTs are damaged by the treatment. Fig. 23A shows a x300k magnification image of a CNT wall, with no visible plasma polymer coating. Fig. 23B shows a x380k magnification image of the curved tip of a CNT, similar to those seen in Fig. 22B. It can be seen that the outer walls of the CNT have been disrupted since the diffraction lines are no longer continuous, unlike in image A. This has been shown to be a result of O_2 plasma treatment [54, 77], so it is likely to also be an effect of the p-type RF treatment.

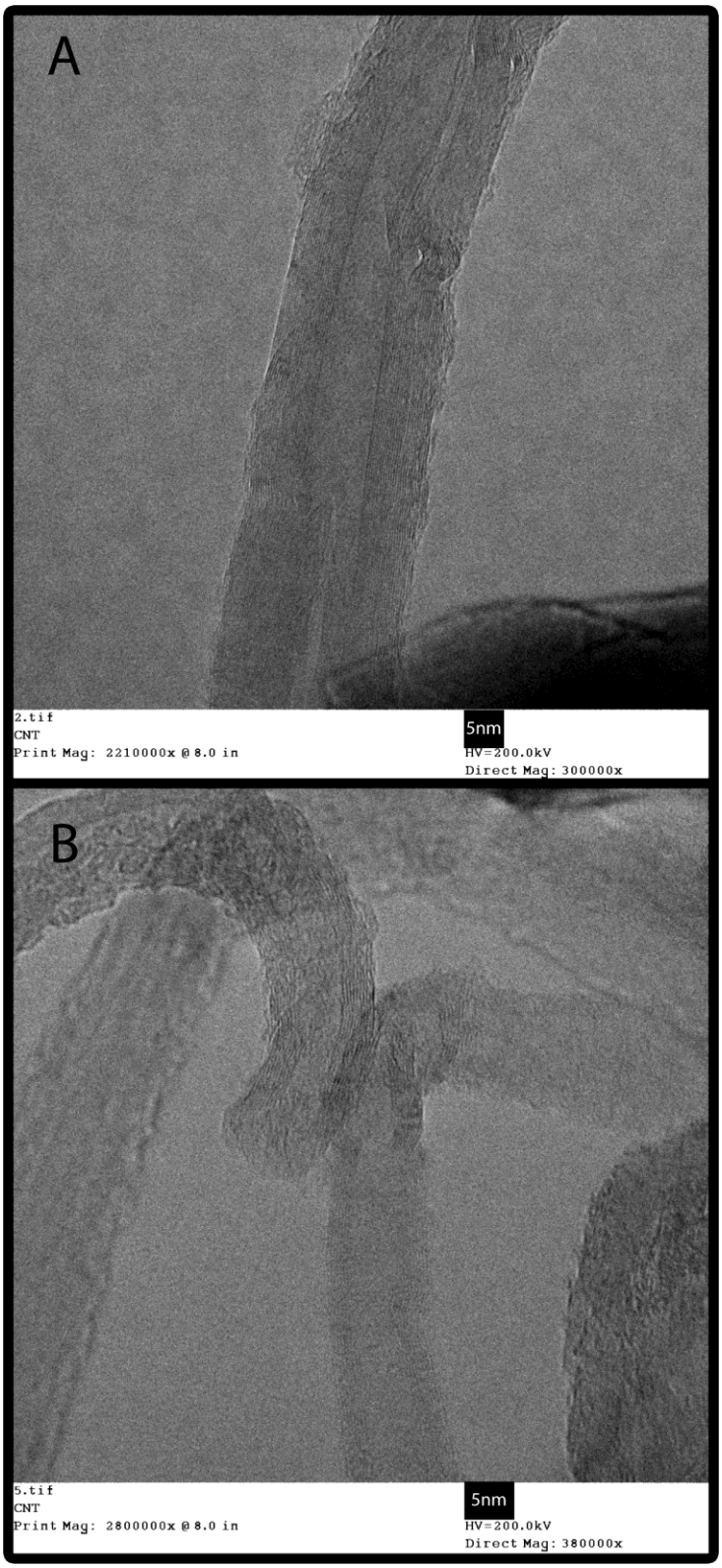

Figure 23: TEM images of 15 min p-treated CNTs. A: x300k CNT showing no deposited plasma polymer layer, B: x380k curled tube end showing damage to outer walls

To conclude the characterization of the p-treated CNTs, a p-treated MWNTs-covered mesh sample was analysed in a transmission mode FTIR before and after p-treatment for 15 min. The two spectra are shown in Figures 24 and 25, respectively. These revealed that chemical changes had occurred to the CNTs. Most noticeable is the presence of a C-H stretch peak spreading from 3000 cm^{-1} to 2750 cm^{-1} in the p-treated sample (Fig. 25), which was absent from the untreated sample (Fig. 24). This could indicate deposition of a saturated plasma polymer coating, which was not seen in the TEM images, or it could also show that the outer walls of the CNTs had been saturated by addition of carbon or hydrogen bonds. The latter hypothesis is supported by the observation that a shift occurred in the position of the noisy region that spreads from 2000 cm^{-1} to 1250 cm^{-1} between the two spectra. There is a shift of the peak at 1275 cm^{-1} in the first spectrum to 1453 cm^{-1} in the second spectrum. The shift can be attributed to a change in the electrical properties of the outer walls of the CNT that occurred during the p-type treatment. As synthesized, CNTs are electrically coupled to the metal substrate from which they grow, causing a change in the electron cloud distribution around the CNTs, and a subsequent shift in the IR absorption [19]. The observed degradation of the outer walls supports this theory, in that an interrupted graphene wall will not conduct electrons as well as a complete one [11, 78]. If this shift is taken into account, the peak at 974 cm^{-1} in Fig. 24 is shifted to 1251 cm^{-1} in Fig. 25 and the peak at 769 cm^{-1} is shifted to 1077 cm^{-1}. In this way, based on peak shape and absorbance values, all peaks observed in Fig. 24 are also visible in Fig. 25, and can be further attributed to sp^2 hybridized carbon from the CNTs, except for the peak at 1453 cm^{-1}, which indicates alkane scissor bending. The peak at 775 cm^{-1} in Fig. 25 is attributed to an alkene bend, which is also an sp^2 hybridized bond and can indicate graphene, and the peak at 958 cm^{-1} is also associated with unsaturated carbon. The presence of oxygen in Fig. 25 appears in the peaks at 1505 cm^{-1}, 1584 cm^{-1}, and 1608 cm^{-1}, which are indicative of carbonyl bonds, and in the numerous peaks between 1000 cm^{-1} and 1200 cm^{-1} for hydroxyl groups. The major peaks seen in the treated sample are summarized in Table 4. Unlike what was observed by Tavares et al, for Cu nanoparticles treated under similar conditions, and in previous studies [16, 79], no strong O-H stretch was observed in the p-treated CNTs. This could be due to the fact that, in the work by Tavares et al, the p-type

treatment was done on KBr powder. KBr is naturally very hydroscopic, so it is possible that exposure to the atmosphere caused the super hydrophilic surface of the p-treated KBr to adsorb moisture from the air. This is supported by the similarity of the FTIR spectrum Swanson et al. collected from a sample treated with lower oxygen concentration to that collected from p-type CNT samples [67]. Finally, the smooth region of the spectra, spreading from approximately 2450 cm^{-1} to 2300 cm^{-1}, is a result of computerized removal of the CO_2 absorbance artefact. In order to automatically adjust the baseline of the spectra, the atmospheric CO_2 peak that is always present was removed by the spectrum analysis software. In general, it is clear from the FTIR data that p-type treatment covalently modified the CNT samples by incorporating polar surface groups into the previously unsaturated graphene walls of the CNTs, without extensive damage to the walls as was seen in pure O_2 and Ar/O_2 studies [53, 54]. This finding is also significant because it explains the previously observed stability of the surface treatment in water contact angle testing.

Table 4: FTIR peak labels for p-treated CNT sample

Peak Location [cm^{-1}]	Strength	Assignment
2962-2826	Strong	Alkane C-H stretch
1608, 1584, 1505	Strong	Carbonyl C=O
1453	Medium	Alkane scissor bend
1251, 1077	Strong	C-O stretch or sp^2 carbon
775	Strong	CNTs

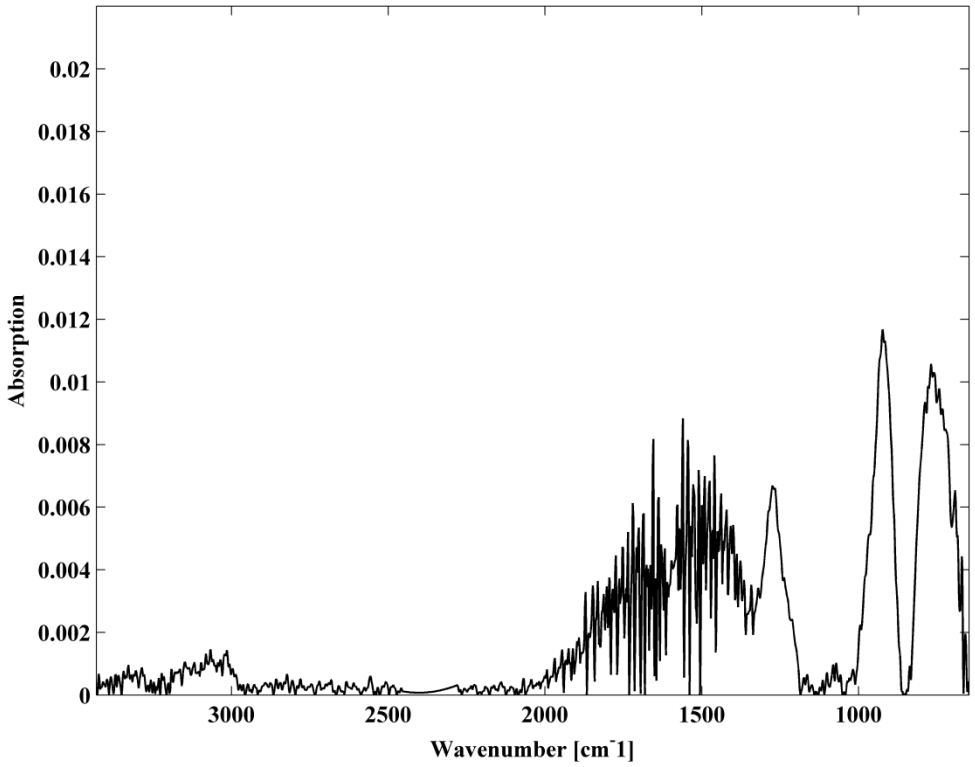

Figure 24: FTIR absorption spectrum of an untreated CNT sample

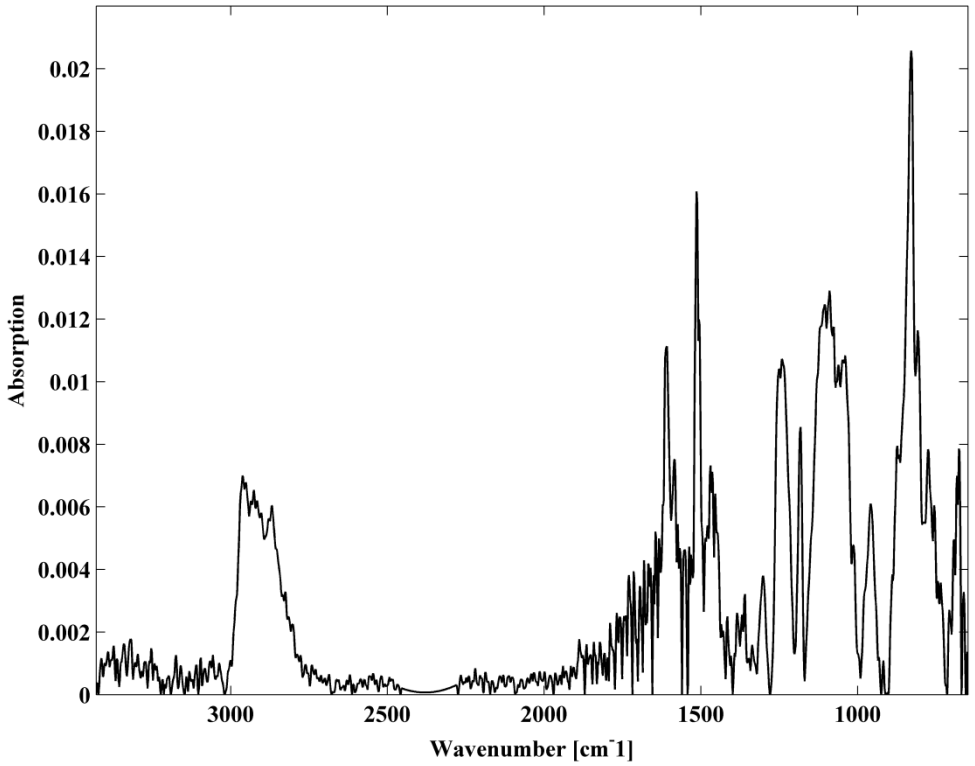

Figure 25: FTIR absorption spectrum of a p-treated CNT sample

5.3 Analysis of Nanofluid Suspensions

Stainless steel substrates with p-type CNT coatings were sonicated at room temperature to prepare aqueous and ethanol suspensions. These were prepared to investigate suspension properties and agglomeration characteristics, respectively. Figure 26 shows three pictures of the 2 dram vials used to make aqueous nanofluid suspensions. Fig. 26A shows a concentrated nanofluid suspension approximately 1 hour after sonication. Fig. 26B and Fig. 26C show a less concentrated nanofluid sample from a different experiment before (B) and after boiling (C) for 20 min. The vial in Fig. 26A was alloquated into two vials; and one was boiled for 20 min. Both were analyzed in the UV-VIS absorption spectrometer and the Z-sizer approximately 1, 2, and 3 hours after preparation. The vial in Fig. 26C was similarly analyzed after boiling, approximately one month after synthesis.

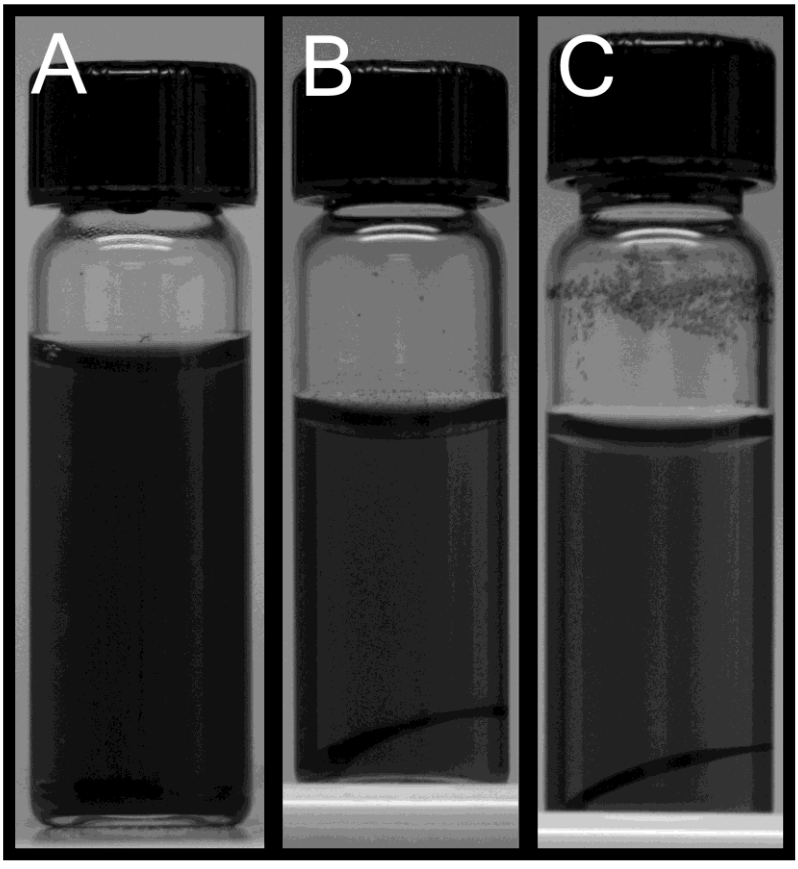

Figure 26: 15 min p-treated CNT nanofluids. A: concentrated sample 1 hour post synthesis, B: low concentration sample 1 hour post synthesis, C: low concentration sample post boiling

An ethanol suspension was prepared by sonication of a p-type CNT sample for 10 min in 5mL of ethanol. The suspension was then sampled and deposited dropwise onto a carbon grid and left to dry. The SEM images shown in Figure 27 are of CNT deposits on the carbon grid. They are deposited on the grid in a flat layer, with no large CNT agglomerate particles present. This shows that the CNTs were not agglomerated in the suspension. The larger particles that are seen in Fig. 27A were found by x-ray analysis to be stainless steel. The report from the EDS system is included as an appendix (A-2).

To characterize the effect of ethanol on the CNTs, the carbon-grid was analyzed in the TEM. There it was found that the CNTs had retained a layer around them, as seen in Figure 28. This coating is actually an artefact of the suspension technique as evidenced by the lack of a similar coating in as-treated CNTs. In the cluster at the center of Fig. 28B, the layer has formed a coherent surface, which was also never seen in TEM analysis of unsuspended p-type CNTs. This artefact occurred due to the nature of the material used to coat the copper TEM grid with a carbon film. The material, called Vinylec®, is a low molecular weight polymer that is slightly soluble in ethanol. It is likely that the dissolved polymer deposited around the p-type CNTs as the ethanol evaporated, leaving a thin polymer coating.

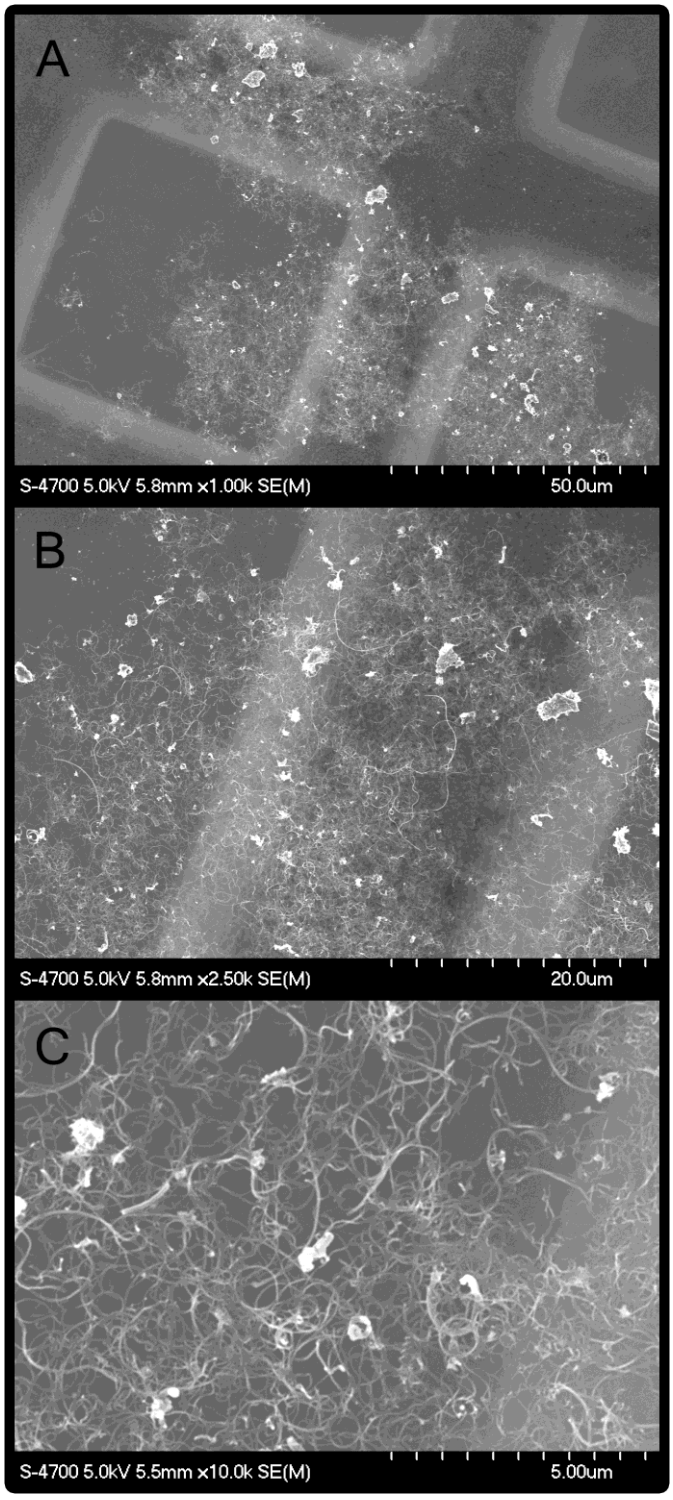

Figure 27: 10 min p-treated CNT deposits sampled from an ethanol nanofluid. A: x1k, B: x2.5k, C: x10k

Figure 28: TEM images of 10 min p-treated CNTs sampled from an ethanol nanofluid showing an ethanol-Vinylec® coating, A: x57k, B: x41k

Analysis of the aqueous suspensions with the Z-sizer revealed that as-prepared and after boiling, the ζ-potential remained consistently negative. An example of one of the plots generated by the Z-sizer is given in Figure 29. The graph shows the ζ-potential of a boiled suspension approximately one month after preparation. Additional graphs for each of the samples tested are presented in the appendix A-1.

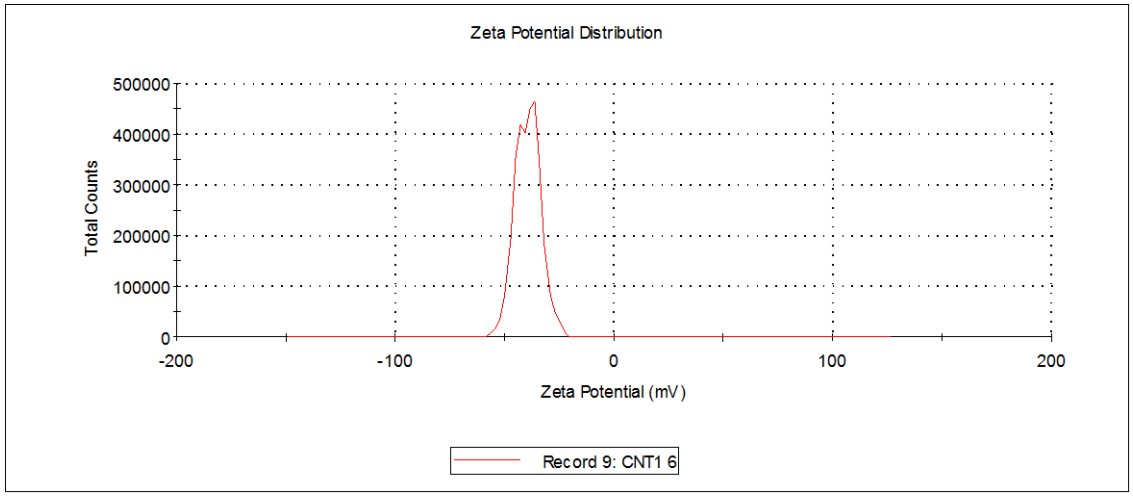

Figure 29: ζ-potential distribution for boiled aqueous p-MWNT nanofluid 1 month post suspension

The ζ-potential values are summarized in Table 5 and Figure 30 below. The values given represent averages of six measurements. Two as-prepared samples and two boiled samples were measured every hour for 3 hours. As-prepared samples tested one, two and three hours after suspension had an average ζ-potential of -34.2 mV with an average standard deviation of 8.9 mV. Boiled samples also showed no change in ζ-potential over the first three hours after preparation. The average ζ-potential for boiled CNT nanofluids was -31.4 mV with an average standard deviation of 6.3 mV. These two distributions overlap to the extent that they are within one standard deviation of each other, so it can be said with confidence that boiling does not affect the ζ-potential of the p-type CNT nanofluid. The average ζ-potential of the boiled CNT nanofluid tested after appromixately one month was -40.3 mV. This higher value can be attributed to differences in the initial CNT growth density, which is thought to have an effect on the efficacy of plasma treatment. The results from this analysis show that not only are the CNT nanofluids stable at room temperature, but they are also not irreversibly altered by

prolonged boiling [72]. This result is especially significant, as previous studies showed suspension degradation after 20 min heating at 69.7°C [9].

Table 5: ζ-potential values for p-treated CNT samples

Sample Time [Post Prep.]	ζ-potential [mV]	Standard Deviation [mV]
As-prepared 1 hour	-33.7	10.2
As-prepared 2 hours	-33.8	10.1
As-prepared 3 hours	-35.1	6.5
1 hour after boiling	-31.8	6.3
2 hours after boiling	-31.4	6.8
3 hours after boiling	-30.9	5.9
1 month after boiling	-40.3	

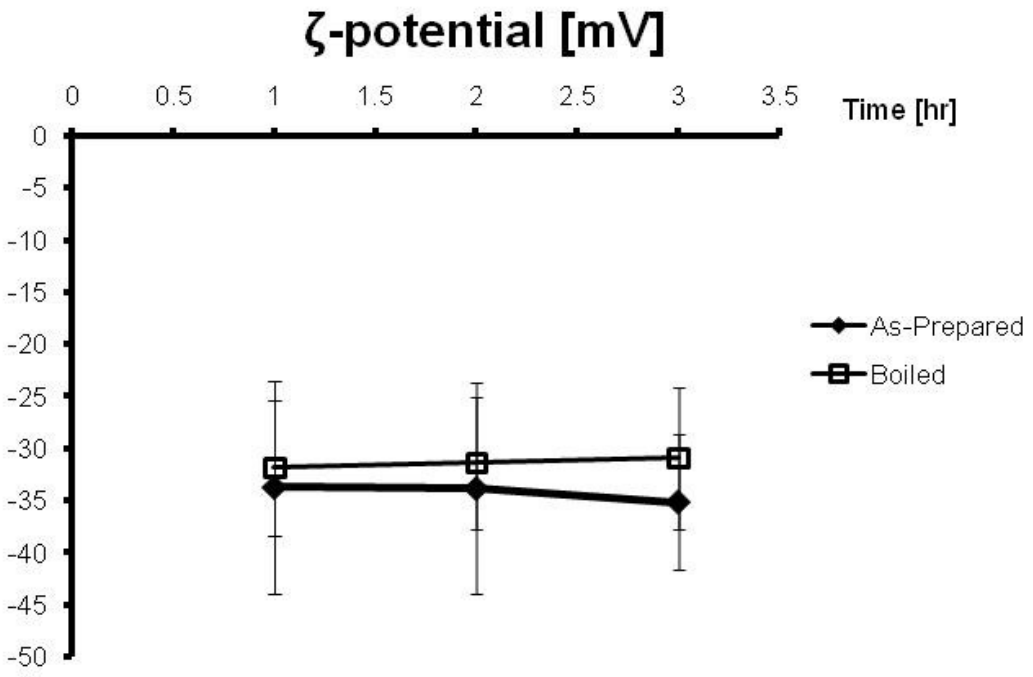

Figure 30: ζ-potential data for boiled and as-prepared p-MWNT nanofluid samples 1, 2, and 3 hours after preparation

UV-VIS absorption spectroscopy analysis supports the data from the Z-sizer. As-prepared aqueous CNT suspensions as well as boiled suspensions were tested one and two hours after preparation and the resulting spectra were compared for change in absorption. Two spectra collected from as prepared and boiled samples are shown in Figure 30 below. There is a slight decrease in absorption for the boiled sample, but because the spectra were measured in relative mode (single bracket), the difference could be an artefact of the measurement. The shape of the spectrum from the boiled CNT nanofluid lends credence to this view, but it can also be attributed to some CNTs agglomerating and settling out of suspension during boiling. The shapes of both curves are characteristic of CNT nanofluids, with the peak in the UV range attributable to the CNTs in suspension [80-82].

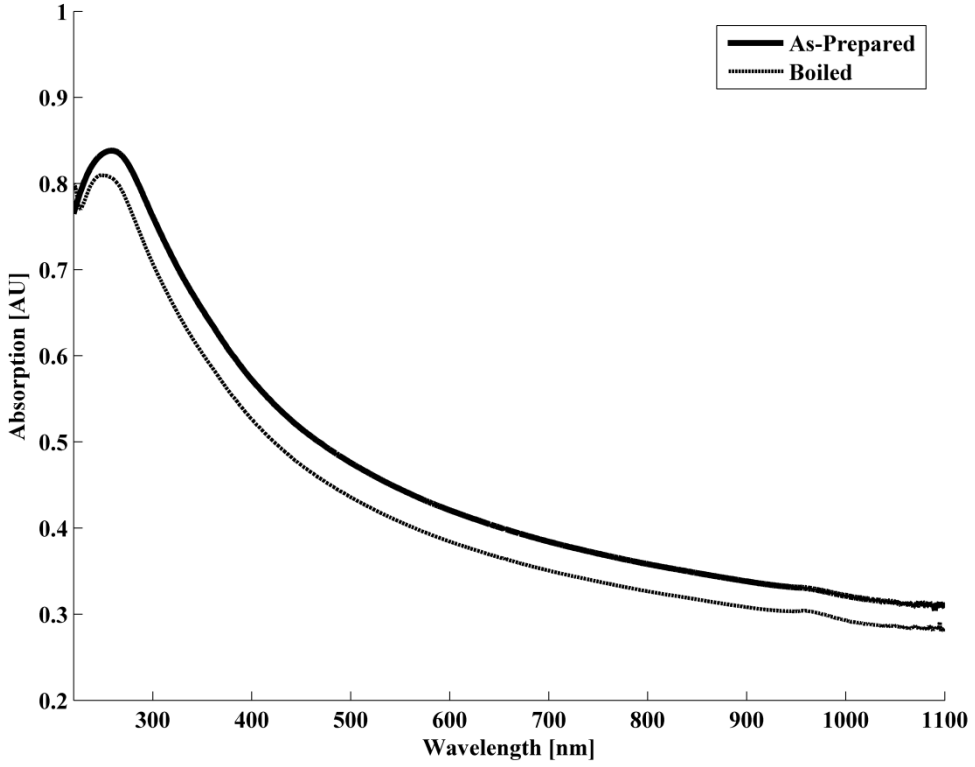

Figure 31: UV-Vis absorption spectrum of as-prepared and boiled p-treated CNT nanofluid 2 hours post suspension

6. Conclusions

6.1 CVD Study

Although no absolute conclusions are to be drawn from this section, the results presented strongly point toward a relationship between surface grain structure and size and CNT growth. The experiments varying the cooling rate between the heat treatment phase and the CNT growth phase of the t-CVD synthesis procedure showed a strong effect on SS304 surface microstructure. In turn, this strongly affected the CNT morphology that developed. Furthermore, an SEM analysis revealed a strong relationship between grain boundaries and CNT growth. Specifically, the presence of crystals grown along grain boundaries prevented CNT growth within a seemingly consistent gap on either side of the grain boundaries. TEM analysis showed that these surface crystals contained very high chromium concentrations, even reaching parity with iron. This leads to the hypothesis that chromium carbide plays an integral role in the growth of CNTs, and therefore suggests the mechanism of carbide nuclei precipitation, also known as sensitization, for producing the active catalyst sites for CNT growth.

6.2 Nanofluids Study

It can be confidently stated that an aqueous CNT nanofluid that is thermally stable up to 100°C was produced by RF glow discharge treatment in $Ar/O_2/C_2H_6$ gas mixtures, as shown by longitudinal ζ-potential measurements on both as-prepared and boiled CNT suspensions. Furthermore, aqueous CNT suspensions did not settle, either before or after boiling. In addition, SEM, FTIR, and TEM analyses showed that the plasma treatment uniformly affects the CNT surfaces, and that by adding oxygen to an ethane-argon plasma, the surface treatment changes from deposition of a non-polar plasma-polymer onto the CNTs to covalent addition of polar groups into the graphene structure of the CNTs. The resulting surface treatments have been shown to significantly modify the surface properties of CNTs in a persistent and stable manner.

7. Future Work

The conclusions drawn from the work on CNT nanofluids are supported by strong evidence, but more data should be gathered about the effect of CNT growth morphology and density on plasma treatment uniformity. To accomplish this, samples of CNTs with different growth densities (i.e. case A vs. case B from Chapter 2) should be treated under identical plasma conditions and then tested for suspension stability. It is hypothesised that higher density CNT samples will be less stable, due to decreased plasma treatment effectiveness.

Furthermore, stable CNT nanofluids should be tested for thermal properties. This project focused on synthesis and stability aspects, but did not investigate any change of thermal properties. It is possible that the oxygen-ethane plasma treatment reduces the electrical conductivity and heat transfer capabilities of the CNTs to the extent that no overall change occurs. This is unlikely, however, because all CNTs observed in the TEM were multi-walled, and multi-walled CNTs are likely to have multiple electrically conductive layers.

Finally, no method has yet been developed to measure the CNT concentration of the nanofluids. This is mostly due to the difficulty of detecting the change in weight of the steel mesh before and after sonication, especially considering that stainless steel particles are also removed. For this reason, it is suggested that a thermo-gravimetric method may be able to measure the CNT content. From this, an average weight concentration could be determined based on the amount of stainless steel mesh that is sonicated and the volume of the nanofluid, as long as the CNT synthesis and plasma treatment methods remain consistent.

References

[1] Miner A, Ghoshal U. Limits of Heat Removal in Microelectronic Systems. IEEE Transactions on Components and Packaging Technologies, 2006;29:743.

[2] Kakac S. Heat Exchangers: Selection, Rating, and Thermal design: CRC Press LLC, 2002.

[3] Bird RB, Stewart WE, Lightfoot EN. Transport Phenomena. Hoboken: John Wiley & Sons, Inc., 2002.

[4] Maxwell JC. A Treatise on Electricity and Magnetism. Oxford: Oxford University Press, 1873.

[5] Wang X-Q, Mujumdar AS. Heat Transfer Characteristics of Nanofluids: A Review. International Journal of Thermal Sciences 2007;46:1.

[6] Das S, Choi S, Patel H. Heat Transfer in Nanofluids A Review. Heat Transfer Engineering 2006;27:3.

[7] Eastman JA, Phillpot SR, Choi SUS, Keblinski P. Thermal Transport in Nanofluids. Annual Review of Materials Research 2004;34:219.

[8] Yu W, Choi SUS. The Role of Interfacial Layers in the Enhanced Thermal Conductivity of Nanofluids: A Renovated Maxwell Model. Journal of Nanoparticle Research 2003;5:167.

[9] Wen D, Ding Y. Effective Thermal Conductivity of Aqueous Suspensions of Carbon Nanotubes (Carbon Nanotube Nanofluids). Thermophysics and Heat Transfer 2004;18:481.

[10] Liqiu W, Xiaohao W. Nanofluids: Synthesis, Heat Conduction, and Extension. Journal of Heat Transfer 2009;131:033102.

[11] Dresselhaus MS, editor Carbon Nanotubes: Synthesis, Stucture, Properties, and Applications. New York: Springer, 2001.

[12] Dresselhaus MS. Phonons in Carbon Nanotubes. Advances in Physics 2000;49:705

[13] Tasis D, Tagmatarchis N, Bianco A, Prato M. Chemistry of Carbon Nanotubes. Chemical Reviews 2006;106:1105.

[14] Uwe Vohrer et al. Plasma Modification of Carbon Nanotubes and Bucky Papers. Plasma Processes and Polymers 2007;4:S871.

[15] Baddour CE, Fadlallah F, Nasuhoglu D, Mitra R, Vandsburger L, Meunier J-L. A Simple Thermal CVD Method for Carbon Nanotube Synthesis on Stainless Steel 304 Without The Addition of An External Catalyst. Carbon 2009;47:313.

[16] Tavares J, E.J. Swanson, S. Coulombe. Plasma Synthesis of Coated Metal Nanoparticles with Surface Properties Tailored for Dispersion. Plasma Processes and Polymers 2008.

[17] Kim UJ, Liu XM, Furtado CA, Chen G, Saito R, Jiang J, Dresselhaus MS, Eklund PC. Infrared-Active Vibrational Modes of Single-Walled Carbon Nanotubes. Physical Review Letters 2005;95:157402.

[18] Ding Y, Alias H, Wen D, Williams RA. Heat Transfer of Aqueous Suspensions of Carbon Nanotubes (CNT Nanofluids). International Journal of Heat and Mass Transfer 2006;49:240.

[19] Lin C-L, Chen C-F, Shi S-C. Field Emission Properties of Aligned Carbon Nanotubes Grown on Stainless Steel Using CH_4/CO_2 Reactant Gas. Diamond and Related Materials 2004;13:1026.

[20] Dai H, Hafner JH, Rinzler AG, Colbert DT, Smalley RE. Nanotubes as Nanoprobes in Scanning Probe Microscopy. Nature 1996;384:147.

[21] Nakayama-Ratchford N, Bangsaruntip S, Sun X, Welsher K, Dai H. Noncovalent Functionalization of Carbon Nanotubes by Fluorescein-Polyethylene Glycol: Supramolecular Conjugates with pH-Dependent Absorbance and Fluorescence. J. Am. Chem. Soc. 2007;129:2448.

[22] Feazell RP, Nakayama-Ratchford N, Dai H, Lippard SJ. Soluble Single-Walled Carbon Nanotubes as Longboat Delivery Systems for Platinum(IV) Anticancer Drug Design. J. Am. Chem. Soc. 2007;129:8438.
[23] Krajcik R, Jung A, Hirsch A, Neuhuber W, Zolk O. Functionalization of Carbon Nanotubes Enables Non-Covalent Binding and Intracellular Delivery of Small Interfering RNA for Efficient Knock-Down of Genes. Biochemical and Biophysical Research Communications 2008;369:595.
[24] Iijima S. Helical Microtubules of Graphitic Carbon. Nature 1991;354:56.
[25] Harris PJF. Carbon Nanotubes And Related Structures: New Materials for the Twenty-First Century. Cambridge: Cambridge University Press, 1999.
[26] Thess A, Lee R, Nikolaev P, Dai H, Petit P, Robert J, Xu C, Lee YH, Kim SG, Rinzler AG, Colbert DT, Scuseria GE, Tomanek D, Fischer JE, Smalley RE. Crystalline Ropes of Metallic Carbon Nanotubes. Science 1996;273:483.
[27] Bower C, Zhu W, Jin S, Zhou O. Plasma-Induced Alignment of Carbon Nanotubes. Applied Physics Letters 2000;77:830.
[28] Kong J, Cassell AM, Dai H. Chemical Vapor Deposition of Methane for Single-Walled Carbon Nanotubes. Chemical Physics Letters 1998;292:567.
[29] Baddour CE, Briens C. Carbon Nanotube Synthesis: A Review. International Journal of Chemical Reactor Engineering 2005;3:1.
[30] Masarapu C, Wei B. Direct Growth of Aligned Multiwalled Carbon Nanotubes on Treated Stainless Steel Substrates. Langmuir 2007;23:9046.
[31] Meyyappan M. Carbon Nanotube Growth by PECVD: A Review. Plasma Sources Science And Technology 2003;12:205.
[32] Vander Wal RL, Hall LJ. Carbon nanotube synthesis upon stainless steel meshes. Carbon 2003;41:659.
[33] Davies JR, editor ASM Specialty Handbook: Stainless Steels. Materials Park, OH: Materials Information Society, 1994.
[34] Khatak HS, Raj B, editors. Corrosion of Austenitic Stainless Steels. New Delhi: Narosa Publishing House, 2002.
[35] Kokawa H, Shimada M, Sato Y. Grain-Boundary Structure and Precipitation in Sensitized Austenitic Stainless steel. JOM Journal of the Minerals, Metals and Materials Society 2000;52:34.
[36] Sedriks Aj. Corrosion of Stainless Steels. New York: John Wiley & Sons, Inc., 1996.
[37] Trillo EA, Murr LE. Effects of Carbon Content, Deformation, and Interfacial Energetics on Carbide Precipitation and Corrosion Sensitization in 304 Stainless Steel. Acta Materialia 1998;47:235.
[38] Beltran R, Trillo EA, Romero RJ, Murr LE, Advani AH, Fisher WW. Combined Effects of Strain and Grain Size on Carbide Precipitation and Sensitization in 304 Stainless Steel. Scripta Metallurgica et Materialia ; Vol/Issue: 30:8 1994:Pages: 1021.
[39] Trillo EA, Beltran R, Maldonado JG, Romero RJ, Murr LE, Fisher WW, Advani AH. Combined Effects of Deformation (Strain and Strain State), Grain Size, and Carbon Content on Carbide Precipitation and Corrosion Sensitization in 304 Stainless Steel. Materials Characterization 1995;35:99.
[40] Arnold MS, Green AA, Hulvat JF, Stupp SI, Hersam MC. Sorting Carbon Nanotubes by Electronic Structure Using Density Differentiation. Nat Nano 2006;1:60.
[41] Kim SH, Zachariah MR. In-Flight Size Classification of Carbon Nanotubes By Gas Phase Electrophoresis. Nanotechnology 2005;16:2149.
[42] Krupke R, Hennrich F, Lohneysen Hv, Kappes MM. Separation of Metallic from Semiconducting Single-Walled Carbon Nanotubes. Science 2003;301:344.

[43] Ulbricht H, Berninger M, Deachapunya S, Stefanov A, Arndt M. Gas Phase Sorting of Fullerenes, Polypeptides and Carbon Nanotubes. Nanotechnology 2008;19:045502.
[44] Andreas H. Functionalization of Single-Walled Carbon Nanotubes. Angewandte Chemie 2002;41:1853.
[45] Boul PJ, Liu J, Mickelson ET, Huffman CB, Ericson LM, Chiang IW, Smith KA, Colbert DT, Hauge RH, Margrave JL, Smalley RE. Reversible Sidewall Functionalization of Buckytubes. Chemical Physics Letters 1999;310:367.
[46] Nikitin A, Ogasawara H, Mann D, Denecke R, Zhang Z, Dai H, Cho K, Nilsson A. Hydrogenation of Single-Walled Carbon Nanotubes. Physical Review Letters 2005;95:225507.
[47] Kannan Balasubramanian MB. Chemically Functionalized Carbon Nanotubes. Small 2005;1:180.
[48] Mickelson ET, Chiang IW, Zimmerman JL, Boul PJ, Lozano J, Liu J, Smalley RE, Hauge RH, Margrave JL. Solvation of Fluorinated Single-Wall Carbon Nanotubes in Alcohol Solvents. Journal of Physical Chemistry 1999;103:4318.
[49] Bandow S, Rao AM, Williams KA, Thess A, Smalley RE, Eklund PC. Purification of Single-Wall Carbon Nanotubes by Microfiltration. Journal of Physical Chemistry 1997;101:8839.
[50] Ham HT, Choi YS, Chung IJ. An Explanation of Dispersion States of Single-walled Carbon Nanotubes in Solvents and Aqueous Surfactant Solutions Using Solubility Parameters. Journal of Colloid and Interface Science 2005;286:216.
[51] F. Balavoine PS. Helical Crystallization of Proteins on Carbon Nanotubes: A First Step towards the Development of New Biosensors. Angew. Chem. Int. Ed. 1999;38.
[52] JB. Kim TP. Nanocomposites of Poly(L-lysine) and Single-Walled Carbon Nanotubes. Polymer International 2007.
[53] Felten A, Bittencourt C, Pireaux JJ, Lier GV, Charlier JC. Radio-frequency Plasma Functionalization of Carbon Nanotubes Surface O_2, NH_3, and CF_4 Treatments. Journal of Applied Physics 2005;98:074308.
[54] Xu T, Yang J, Liu J, Fu Q. Surface Modification of Multi-Walled Carbon Nanotubes by O_2 Plasma. Applied Surface Science 2007;253:8945.
[55] Hou Z, Cai B, Liu H, Xu D. Ar, O_2, CHF_3, and SF_6 Plasma Treatments of Screen-Printed Carbon Nanotube Films for Electrode Applications. Carbon 2008;46:405.
[56] Felten A, Bittencourt C, Colomer JF, Van Tendeloo G, Pireaux JJ. Nucleation of Metal Clusters on Plasma Treated Multi Wall Carbon Nanotubes. Carbon 2007;45:110.
[57] Bishun NK, Meyyappan M, Joel K, Patrick W, Metagus S, Hiroshi I, Jessica K, Charles W. Baushchlicher, Jr. A Glow-Discharge Approach for Functionalization of Carbon Nanotubes. Applied Physics Letters 2002;81:5237.
[58] Li P, Lim X, Zhu Y, Yu T, Ong C-K, Shen Z, Wee AT-S, Sow C-H. Tailoring Wettability Change on Aligned and Patterned Carbon Nanotube Films for Selective Assembly. The Journal of Physical Chemistry B 2007;111:1672.
[59] Gamal A, Pagona P, Ganjigunte RSI, Ian WK, Li CC. Substitutional Nitrogen Incorporation Through RF Glow Discharge Treatment And Subsequent Oxygen Uptake On Vertically Aligned Carbon Nanotubes. Physical Review B (Condensed Matter and Materials Physics) 2007;75:195429.
[60] Plank NOV, Liudi J, Cheung R. Fluorination of carbon nanotubes in CF_4 plasma. Applied Physics Letters 2003;83:2426.
[61] Donglu S, Jie L, Peng H, Wang LM, Feng X, Ling Y, Mark JS, David BM. Plasma Coating Of Carbon Nanofibers For Enhanced Dispersion And Interfacial Bonding In Polymer Composites. Applied Physics Letters 2003;83:5301.

[62] Donglu S, Jie L, Peng H, Wang LM, Wim JvO, Mark S, Yijun L, David BM. Plasma Deposition Of Ultrathin Polymer Films On Carbon Nanotubes. Applied Physics Letters 2002;81:5216.
[63] Novák I, Florián Š. Investigation Of Long-Term Hydrophobic Recovery Of Plasma Modified Polypropylene. Journal of Materials Science 2004;39:2033.
[64] Cosgrove T, editor Colloid Science: Principles, Methods, And Applications: Blackwell Publishing, 2005.
[65] Liu M-S, Lin MC-C, Tsai CY, Wang C-C. Enhancement Of Thermal Conductivity With Cu For Nanofluids Using Chemical Reduction Method. International Journal of Heat and Mass Transfer 2006;49:3028.
[66] Lee D, Kim J-W, Kim BG. A New Parameter to Control Heat Transport in Nanofluids: Surface Charge State of the Particle in Suspension. The Journal of Physical Chemistry B 2006;110:4323.
[67] Swanson EJ. Dual-Plasma Synthesis Of Coated Metal Nanoparticles With Controlled Surface Properties. Chemical Engineering. M.Eng. Montreal: McGill University, 2008.
[68] de Gennes PG. Wetting: Statics And Dynamics. Reviews of Modern Physics 1985;57:827.
[69] P. G, de Haseth JA. Fourier Transform Infrared Spectrometry. Hoboken: Wiley-Interscience, 2007.
[70] Skoog DA, Holler J, Crouch SR. Principles of Instrumental Analysis: Brooks Cole, 2006.
[71] ASTM. Zeta Potential Of Colloids In Water And Waste Water. D 4187-82, 1985.
[72] Castro M, Al-Dahoudi N, Oliveira P, Schmidt H. Multi-Walled Carbon Nanotube-Based Transparent Conductive Layers Deposited On Polycarbonate Substrate. Journal of Nanoparticle Research.
[73] Deck CP, Vecchio K. Prediction Of Carbon Nanotube Growth Success By The Analysis Of Carbon-Catalyst Binary Phase Diagrams. Carbon 2006;44:267.
[74] Nasibulin AG, Pikhitsa PV, Jiang H, Kauppinen EI. Correlation Between Catalyst Particle And Single-Walled Carbon Nanotube Diameters. Carbon 2005;43:2251.
[75] Larsson P, Larsson JA, Ahuja R, Ding F, Yakobson BI, Duan H, Rosen A, Bolton K. Calculating Carbon Nanotube--Catalyst Adhesion Strengths. Physical Review B (Condensed Matter and Materials Physics) 2007;75:115419.
[76] Coleman JN, Khan U, Blau WJ, Gun'ko YK. Small But Strong: A Review Of The Mechanical Properties Of Carbon Nanotube-Polymer Composites. Carbon 2006;44:1624.
[77] Felten A, Ghijsen J, Pireaux J-J, Johnson RL, Whelan CM, Liang D, Tendeloo GV, Bittencourt C. Effect Of Oxygen Rf-Plasma On Electronic Properties Of CNTs. Journal of Physics D: Applied Physics 2007;40:7379.
[78] Roy SS, Papakonstantinou P, Okpalugo TIT, Murphy H. Temperature Dependent Evolution Of The Local Electronic Structure Of Atmospheric Plasma Treated Carbon Nanotubes: Near Edge X-Ray Absorption Fine Structure Study. Journal of Applied Physics 2006;100:053703.
[79] Le Dû G, Celini N, Bergaya F, Poncin-Epaillard F. RF Plasma-Polymerization Of Acetylene: Correlation Between Plasma Diagnostics And Deposit Characteristics. Surface and Coatings Technology 2007;201:5815.
[80] Kataura H. Optical Properties of Single-Wall Carbon Nanotubes. Synthetic Metals 1999;103:2555.
[81] Spataru CD. Excitonic Effects and Optical Spectra of Single-Walled Carbon Nanotubes. Physics Review Letters 2004;92.
[82] Dice GD, Mujumdar S, Elezzabi AY. Plasmonically Enhanced Diffusive And Subdiffusive Metal Nanoparticle-Dye Random Laser. Applied Physics Letters 2005;86:131105.

Appendix

A-1. ζ-potential Distribution Curves

Appendix Figure 1: As-Prepared P-treated CNT Nanofluid, First Measurement

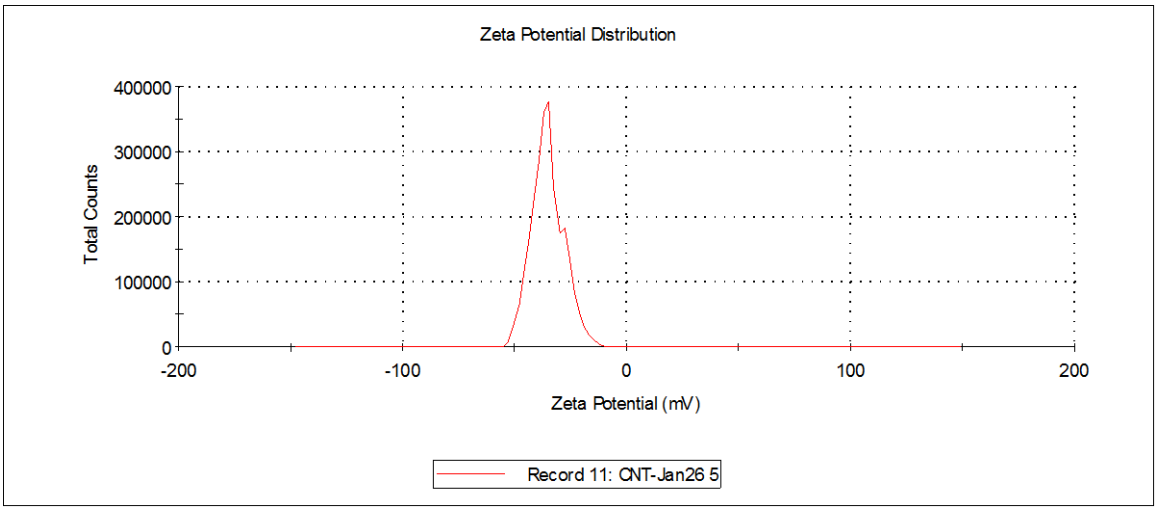

Appendix Figure 2: As-Prepared P-treated CNT Nanofluid, Second Measurement (1 hour)

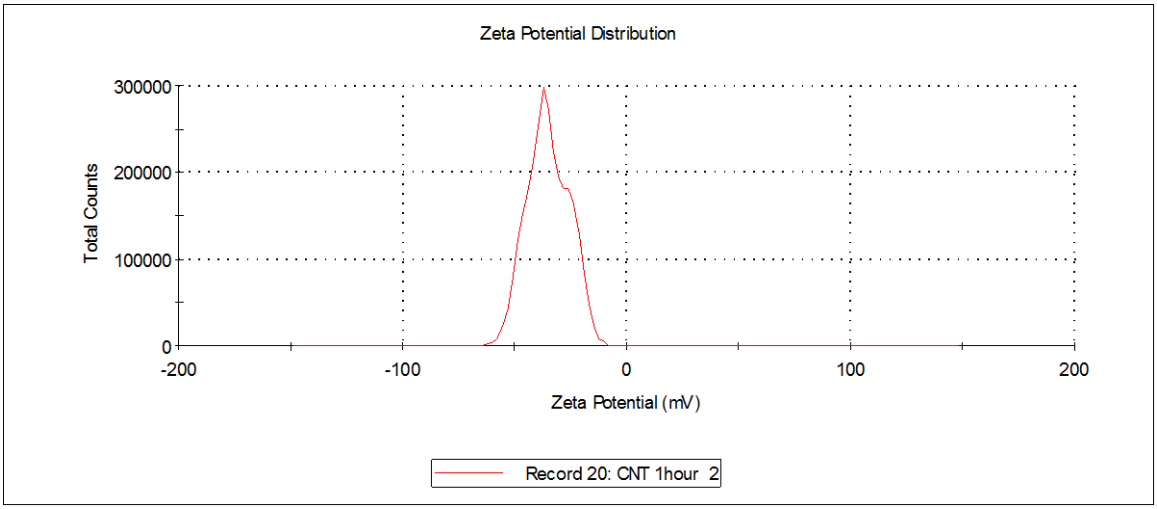

Appendix Figure 3: As-Prepared P-treated CNT Nanofluid, Second Measurement (2nd hour)

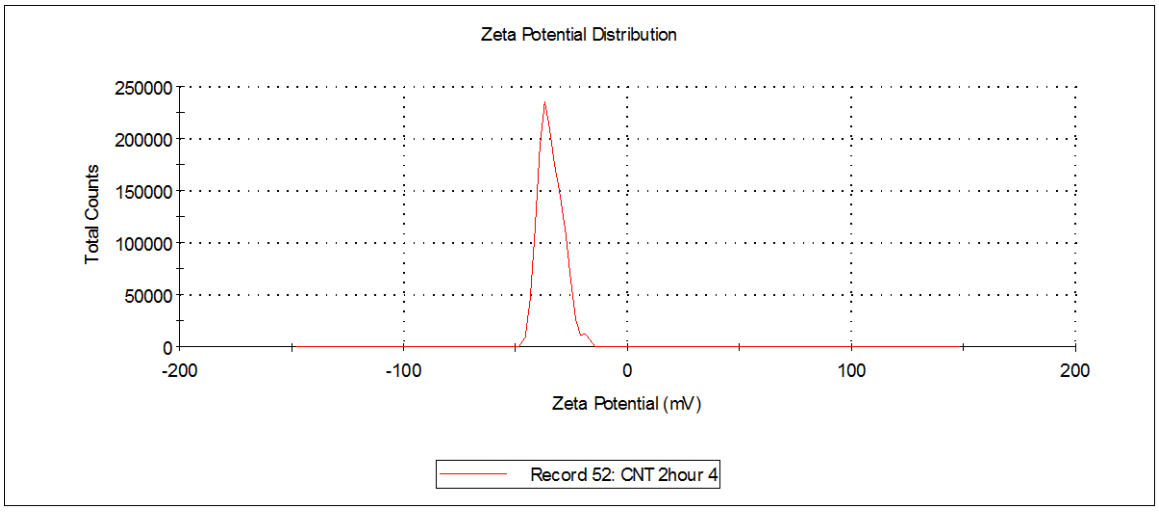

Appendix Figure 4: Boiled P-treated CNT Nanofluid, First Measurement (1st hour)

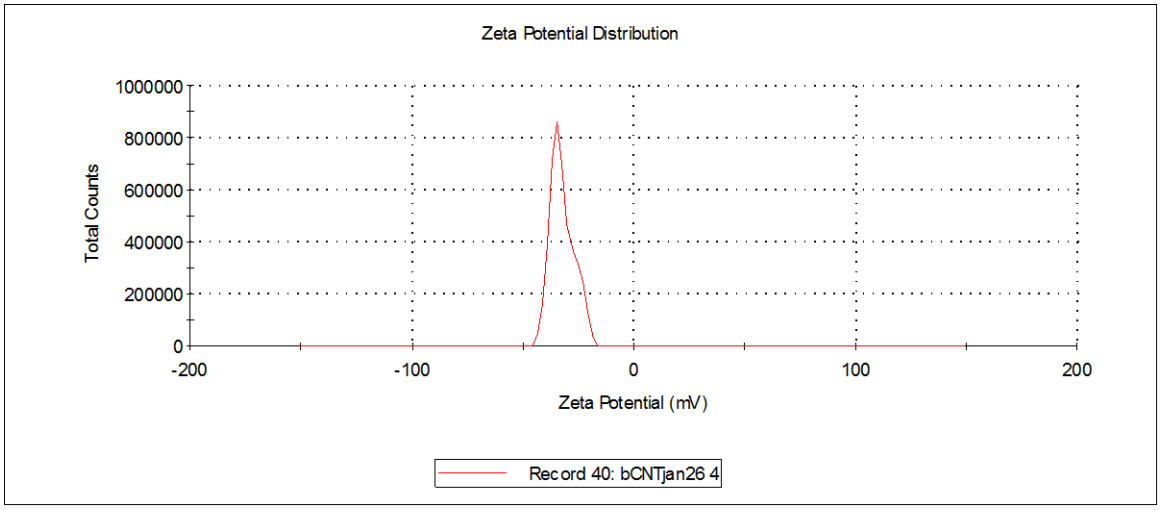

Appendix Figure 5: Boiled P-treated CNT Nanofluid, Second Measurement (2nd hour)

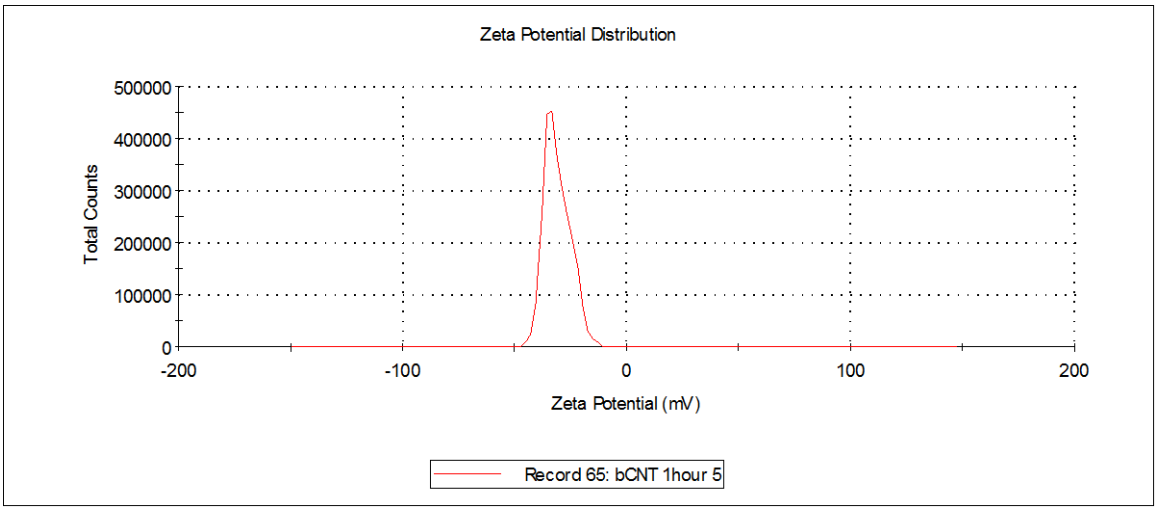

Appendix Figure 2: Boiled P-treated CNT Nanofluid, Third Measurement (3rd hour)

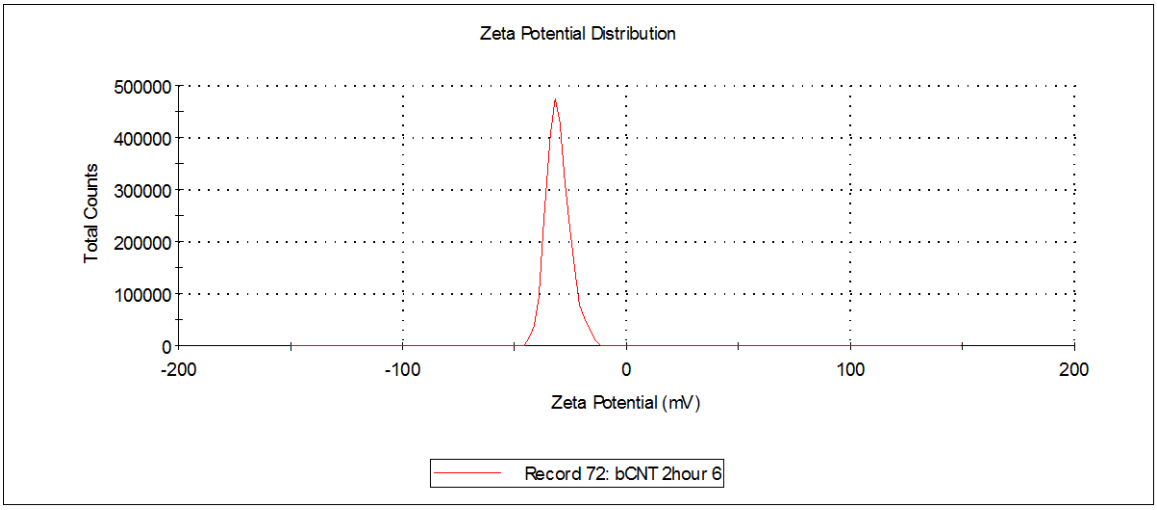

A-2. EDS Report Printout

Project 1

10/12/2008 16:01:44

Spectrum processing :
Peak possibly omitted : 3.660 keV

Processing option : All elements analyzed (Normalised)
Number of iterations = 5

Standard :
C CaCO3 1-Jun-1999 12:00 AM
O SiO2 1-Jun-1999 12:00 AM
Al Al2O3 1-Jun-1999 12:00 AM
Cr Cr 1-Jun-1999 12:00 AM
Mn Mn 1-Jun-1999 12:00 AM
Fe Fe 1-Jun-1999 12:00 AM
Cu Cu 1-Jun-1999 12:00 AM

Element	Weight%	Atomic%
C K	18.31	35.54
O K	26.59	38.74
Al K	4.66	4.03
Cr K	26.81	12.02
Mn K	4.99	2.12
Fe K	14.15	5.91
Cu L	4.48	1.64
Totals	100.00	

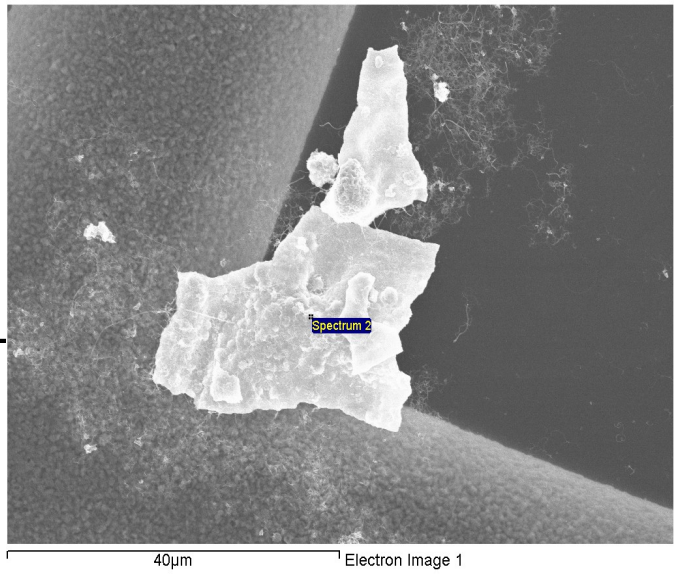

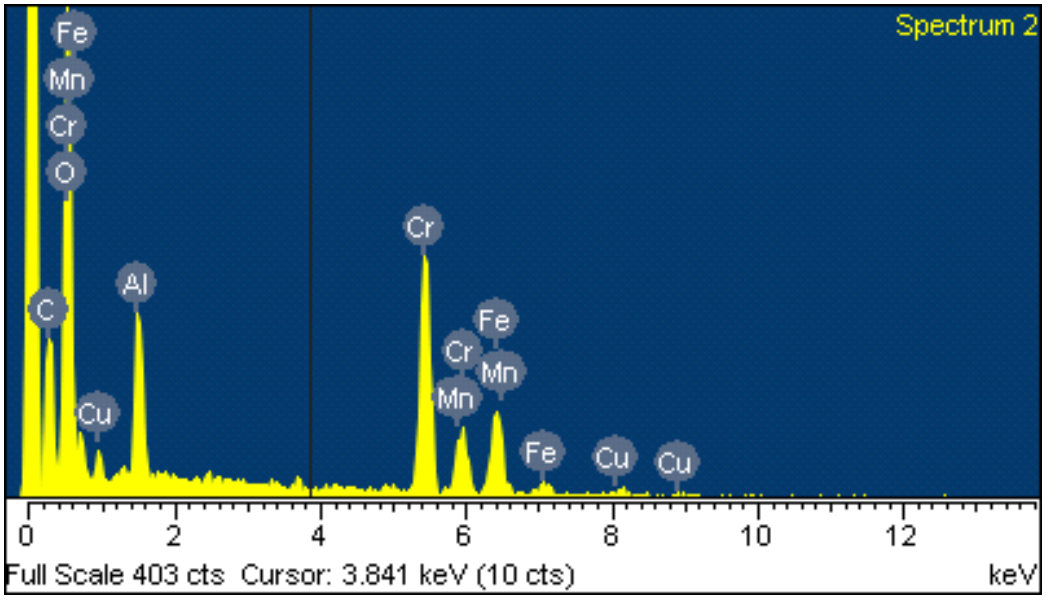

Comment: